

Heralded photonic graph states with inefficient quantum emitters

Maxwell Gold,^{1,*} Jianlong Lin,^{2,*} Eric Chitambar,² and Elizabeth A. Goldschmidt^{1,†}

¹*Department of Physics, University of Illinois Urbana-Champaign, Urbana, IL 61801*

²*Department of Electrical and Computer Engineering,
University of Illinois Urbana-Champaign, Urbana, IL 61801*

(Dated: October 1, 2024)

Quantum emitter-based schemes for the generation of photonic graph states offer a promising, resource efficient methodology for realizing distributed quantum computation and communication protocols on near-term hardware. We present a heralded scheme for making photonic graph states that is compatible with the typically poor photon collection from state-of-the-art coherent quantum emitters. We demonstrate that the construction time for large graph states can be polynomial in the photon collection efficiency, as compared to the exponential scaling of current emitter-based schemes, which assume deterministic photon collection. The additional overhead to achieve this advantage consists of an extra spin system plus one additional spin-spin entangling gate per photon added to the graph. While the proposed scheme enables the generation of graph states for arbitrary applications, we show how it can be further simplified for the specific task of measurement-based computation, leading to significantly higher rates and removing the need for photonic memory in certain computations. As an example use-case of our scheme, we construct a protocol for secure two-party computation that can be implemented efficiently on current hardware. Estimates of the fidelity to produce graph states used in the computation are given, based on current trapped ion experimental benchmarks.

I. INTRODUCTION

The vast promise of quantum information technologies for faster and more secure computational and information systems relies on entanglement as a primary resource. Traditional gate-based quantum computing requires the ability to perform sequences of joint operations across multiple qubits. An alternative paradigm, known as measurement-based quantum computation (MBQC), realizes universal computation through sequences of single qubit measurements made on an initially prepared entangled resource state [1]. This is an appealing approach for photonic quantum systems as single photon rotations and measurements are straightforward using commercial optical elements, and fast efficient routing solutions are readily available [2]. Furthermore, the sequential nature of photon emission allows entangled states to be built from photons emitted at different times by the same emitter [3]. By using entangled emitters, it then becomes possible to simulate entangling gates between photons and overcome the difficulty of realizing direct photon-photon interactions [4]. Indeed, it is known that computationally useful graph states of photons can be generated using either a small number of coherent quantum emitters [5], a combination of a single emitter and fusion gates [6–8], or a single quantum emitter in a feedback scheme [9].

All of these aforementioned schemes assume a photon is successfully added to the graph every time an emitter is excited, and we thus term this class of schemes as being “deterministic”. However, efficient collection

from individual quantum emitters is a challenge that remains largely out of reach today, making deterministic schemes impractical for generating large graph states on even near-term hardware [10].

We introduce a procedure for building arbitrary photonic graph states using a single emitting spin and a fixed number of auxiliary spins, without any requirement on the collection efficiency of the emitted photons. The rate and size of feasible graph states generated by the proposed method has polynomial dependence on the collection efficiency, compared to the exponential suppression of the feasible graph size for the successive detection of photons required in current deterministic schemes. This enhanced performance is achieved by recognizing the possibility of adding each photon to the graph only after successful spin-photon entanglement generation has been heralded.

In Section II of this work, we describe a non-destructive method for this heralding that is implementable on current hardware by swapping the entanglement to another photon, termed the herald-on-swap (HoS) method. More generally, any non-destructive detection of the photon would be suitable to implement this “emit then add” method of building graphs for arbitrary use. We explain in Section III how we can herald on destructive detection of the photon for certain graph state protocols, including MBQC. This enables much higher production rates and fidelities than any currently feasible non-destructive heralding method. In this case, the emitted photon is measured prior to adding it to the graph, thereby abrogating the need for entanglement swapping or photon storage, and dramatically speeding up graph construction. In this case, the graph state is built only virtually as every photon in the graph is necessarily measured. We refer to this as a herald-on-detection (HoD) method,

* These two authors contributed equally

† goldschm@illinois.edu

and Section III provides more detail on when the HoD method can be applied.

In both the HoS and HoD schemes we propose, the photons are emitted over a longer time, when compared to other emitter-based methods for building photonic graph states; this is because most attempts to add a photon to the graph will result in an unsuccessful herald. Consequently, it is the number of excitation attempts that can be made during the coherence time of the emitter that sets the practical limit on the graph size, rather than the collection efficiency. Trapped neutral atoms and ions in vacuum are well suited to this scheme as they exhibit long coherence times ($10^0 - 10^3$ seconds) [11, 12] and host high-fidelity deterministic entangling gates ($> 99\%$) [13–15] with moderate collection efficiencies ($\gtrsim 10\%$ with high-NA optics and $\gtrsim 40\%$ with parabolic reflectors) [16–19]. Higher collection can be achieved by coupling emitters to high quality resonators, but this introduces additional challenges for implementing high-fidelity entangling gates (necessary for generating the higher dimensional graph states required for MBQC) and dramatically reduces the bandwidth of operation [20, 21]. Even higher collection efficiency has been shown with quantum dot sources [7, 22], but in these systems high-fidelity entangling gates between spins are still out of reach and spin coherence times are orders of magnitude shorter than atoms and ions. We also note that some solid-state systems, such as rare-earth emitters, can exhibit excellent coherence, spin-spin entangling gates, and reasonable photon collection via integration into photonic devices [23]. In Section IV we provide estimates of the rate and fidelity for the production of heralded graph states via both of our schemes assuming state-of-the-art trapped ion and photon pair source architectures, which include realistic sources of loss, noise, and decoherence.

Lastly, in Section V we propose a protocol for performing secure two-party classical computation, in which two parties privately compute a function of their input variables with the help of a Referee. Compared to universal quantum computation, our protocol only requires Pauli measurements, and so the entire procedure can be performed using only our HoD method. We demonstrate how secure two-party computation can be achieved using just a single quantum emitter and two auxiliary spin qubits, regardless of the size of the party’s input. We provide fidelity estimates to produce the graph states required for our protocol on current hardware, which suggests this is a highly feasible use-case for quantum networks in the near term. A security analysis is provided to demonstrate how a party can keep their input private. In addition we discuss the resulting bit error rates of the protocol that can be achieved with and without classical error correction.

II. SPIN-PHOTON ENTANGLEMENT SCHEMES

We first describe the HoS scheme, shown in Figure 1, for making graph states for arbitrary applications. Given the technical challenges associated with photon non-demolition measurement [24], this swapping step is required to herald without destructive measurement of the photonic qubit on near-term hardware. Compared to the deterministic scheme described in [5], we include a local entanglement swapping step between an emitter-photon entangled pair and a pair of entangled photons, and only add the final photon to the graph upon success of that swap. A single emitter is initialized onto an unentangled state and excited to produce a single photon that is entangled with its long-lived internal spin state and collected with some overall efficiency η_e . This can be implemented with a wide variety of quantum emitters including laser-cooled atoms or ions, quantum dots, and defects or dopants in wide-bandgap semiconductors [3, 10, 25–27]. Photons can be encoded in various degrees of freedom including polarization, time-bin, and frequency [28–32]. Simultaneously, a pair of entangled photons is probabilistically produced, which can be implemented via standard nonlinear optical processes, such as spontaneous parametric down conversion (SPDC) [33, 34]. One member of the photon pair, the signal photon, is wavelength and bandwidth matched to the emitter photon, and the entangled pair is encoded in the same degree of freedom as the emitter photon. The emitter photon and signal photon are sent to a joint measurement apparatus which, upon a successful measurement outcome, projects the emitter spin and the unmeasured photon, the idler photon, onto an entangled Bell state [35]. Since only certain measurement outcomes correspond to entanglement between the emitter spin and idler photon, and imperfect collection and detection means that fewer than two photons are detected on most attempts, the procedure is repeated until a successful herald is flagged. Following each failed attempt, the emitter is measured and reinitialized for the subsequent attempt at a successful herald.

We assume the emitter is among a set of spin qubits that can be controllably entangled in a pair-wise way via local and deterministic two-qubit spin-spin entangling gates, such as an array of trapped atomic ions or neutral atoms. Upon a successful herald, the emitter spin is deterministically entangled with an auxiliary spin, which may already be part of a larger graph state. The emitter spin is then rotated to a conjugate basis and projectively measured, removing it from the graph without disturbing any of the other qubits. Following a correction to the photon based on the outcome of this measurement, the state of the system is as if the auxiliary spin had directly emitted the photon itself. This “emit then add” method then allows for the construction of arbitrary photonic graph states using the methods described in [5]. Namely, the graph states are built using sequences of two-qubit gates on the spins and local Clifford gates on

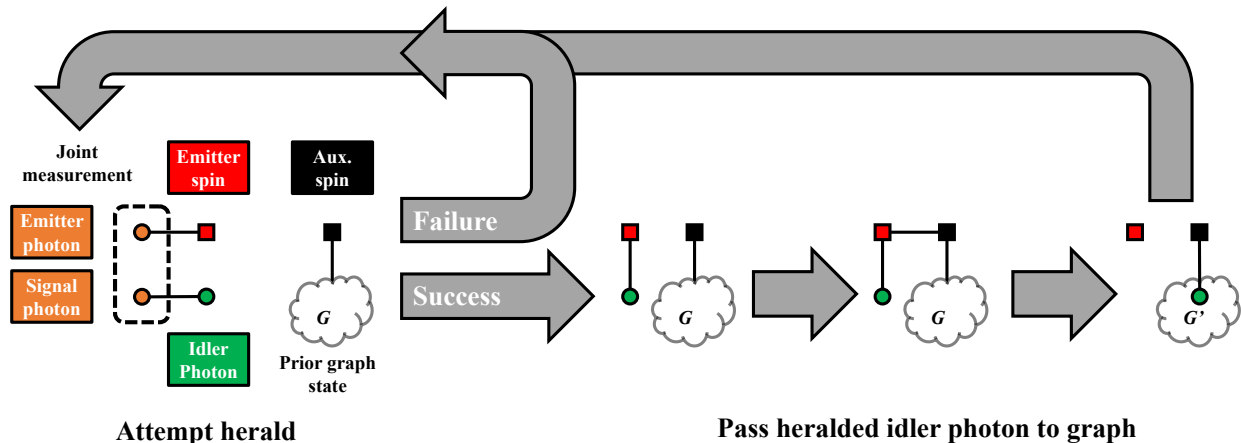


FIG. 1. Heraldon-Swap (HoS) scheme. The components are two initial entangled pairs: an emitter spin (red square) entangled with a photon (orange circle) and a signal-idler entangled photon pair (orange and green circle, respectively). We also assume an existing graph G that contains one or more auxiliary spins (black square). Entanglement swapping is attempted between the two initial entangled pairs. Upon success, a two-qubit spin-spin gate deterministically entangles the emitter spin and auxiliary spin. A local complementation operation is then performed on the emitter spin, which is subsequently measured out of the graph. This leaves the idler photon a part of the graph and the emitter spin reinitialized for the next attempted emission.

the photons. The local gates on each photon can all be combined and applied as a single rotation prior to using the graph state in subsequent applications.

The key improvement in our scheme is that the idler photon can be collected with near unit efficiency upon a successful herald [36]. Attaining the improvement of this scheme requires one additional two-qubit spin-spin entangling gate per photon added to the graph plus one additional spin (the emitter), compared to the requirements for generating graphs via known deterministic schemes [37]. In addition, the graph is emitted over a much longer time and thus requires longer spin coherence times. We note an additional benefit of the scheme in that the idler photon can be at virtually any wavelength due to the flexibility of standard entangled photon pair sources [38–41], which overcomes common challenges due to the inconvenient emission colors of many atomic qubits. We show here that current state-of-the-art trapped ion systems can be designed to produce graph states of tens to hundreds of photons using the proposed method, where extending to thousands would be made possible with reasonable improvements [12, 14, 16].

III. A HERALDING SCHEME FOR MBQC

The HoS scheme described in the previous section, or any other non-destructive heralding of successful collection of the emitter photon, can be used to build arbitrary photonic graph states. We show in this section that for many applications, including MBQC, non-destructive measurement is not required. For these applications the nodes are measured sequentially with the choice of mea-

surement basis on one node depending on outcomes of previous ones. It is, thus, not necessary to build the full graph state before beginning these measurements [42]. Instead, an emitted photon can be destructively measured as soon as the correct basis for measurement is determined. This measurement thus serves doubly as a prescribed step in the MBQC protocol and as a way for detecting the emitted photon. Upon failure to detect the photon, we reinitialize the emitter and attempt generation again, having left the larger graph undisturbed, as in the HoS scheme. Upon successful detection, we perform all required gates on the emitter and auxiliary spins, measure the emitter out of the graph, and reinitialize the emitter to attempt generation of the next photon in the graph.

This simpler HoD scheme is shown in Figure 2, and it has the advantage that it requires no storage time for the emitted photon prior to measurement. There are limitations for when this scheme can be employed. Namely, a photon can be measured using HoD provided the two conditions are satisfied: (1) the correct measurement basis for that photon, as set by the MBQC protocol, is determined prior to its emission, and (2) this measurement is either Pauli Z or of the form $\cos \phi X + \sin \phi Y$. Condition (1) can be met in general, as the emission order can be chosen to match the measurement order of the computation, albeit at the cost of using extra auxiliary spins and two-qubit gates in some cases [37]. The second condition can also be met in principle, since the specified gate sets are sufficient for universal MBQC [1, 43].

To understand condition (2) in more detail, note that if the full graph state were built using HoS and two-qubit gates on the auxiliary spins, then each emitted photon

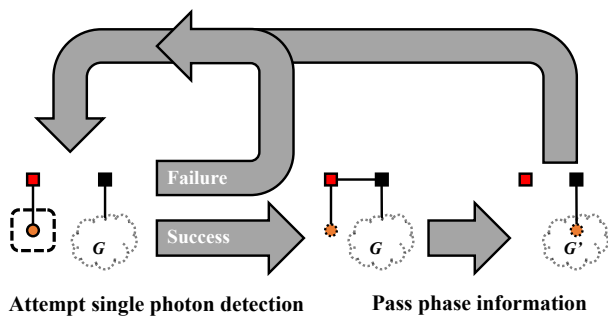


FIG. 2. Heralded-on-detection (HoD) scheme. For certain MBQC protocols, it is sufficient to perform the deterministic entangling gate between the emitter and auxiliary spin only upon successful detection of the emitted photon. The photonic graph state constructed in this case is virtual (represented by dashed boundaries) and exists as a set of conditional phases stored on the auxiliary spin(s).

would have a local Clifford error of the form UZ^m , where U is a fixed Clifford and $m \in \{0, 1\}$ is determined by the decoupling measurement on the emitter spin. If M is the measurement to be subsequently performed on the photon in the MBQC protocol, then when correcting for the Clifford error, the effective measurement would be $M' = UZ^mMZ^mU^\dagger$. When $M = Z$, then $M' = UZU^\dagger$; or when $M = \cos \phi X + \sin \phi Y$, then $M' = (-1)^m UZU^\dagger$. In the first case, the dependence on m is completely removed, and the photon can be equivalently measured with UZU^\dagger immediately after it is emitted in the HoD scheme. In the second case, it can also be immediately measured with UZU^\dagger , but now one must perform a bit flip on the classical measurement outcome if $m = 1$; this is because an overall -1 factor on a spin observable simply flips the spin-up/spin-down outcomes. In summary, the correct computation can be attained through HoD and classical post-processing for observables of the specified form.

While satisfying conditions (1) and (2) above is sufficient for universal MBQC using HoD, this is often not the most efficient method in terms of the overall number of photons used to drive the computation. For example, building out the graph to a certain depth and measuring in a different sequence than the emission order can lead to more compact gate implementations [43]. Also, using MBQC measurements outside of the x-y plane allows for more general forms of information flow [44]. Nevertheless, as we show in the next section, the HoD scheme can enable dramatically faster construction and higher fidelity with no photon storage required. For the HoS (or any non-destructive heralding) scheme, photon storage is required for at least the time to perform the spin-spin entangling gates and the decoupling measurement on the emitter.

IV. SCALING AND FIDELITY FOR HERALDED SCHEMES

A major benefit of both schemes comes in scaling up the size of graph states using near term hardware. The average time to successfully generate an n_p -photon graph by directly collecting photons from an emitter in n_p subsequent excitation events for computation is $\mathcal{O}(\eta_e^{-n_p})$, where η_e is the emitter collection efficiency, as any failed detection event truncates the graph. In typical deterministic quantum emitter-based schemes, any inefficiency in collection therefore leads to exponentially bad scaling with graph size. Given current hardware, this severely limits the size and rate of generation for photonic graph states, particularly those that require multiple spin qubits. We note that there are loss tolerance and percolation thresholds that improve this scaling, but they require much better collection efficiency than is feasible in near-term systems [45–48]. For the heralded schemes, any failed detection of the emitter photon simply results in the reinitialization of the emitter and another attempt at the joint or single photon detection, while the graph under construction remains unaffected. Therefore, an n_p -photon graph state will be created over a time that is $\mathcal{O}(n_p \eta_e^{-1})$. As a comparison, the time to make an n_p -photon graph state (in units of the repetition period) is shown in Figure 3 for $\eta_e \in \{0.1, 0.25, 0.4\}$ for the deterministic (red), HoS (blue), and HoD (yellow) schemes. We do not include the time to perform gates and measurements on the spins for these estimates, and we assume that the emitter coherence does not limit the graph size for the deterministic scheme ($n_p/\tau R_{\text{rep}} \ll 1$ where τ is the spin coherence time and R_{rep} is the repetition rate of excitation). In practice, however, the short coherence times of the most efficient photon emitters further limit the size of graphs that can be produced in the deterministic scheme [10, 32]. For the heralded schemes, all auxiliary spins must remain coherent for the entire time they are a part of the graph, which is much longer than the n_p repetition cycles over which the graph is generated in the deterministic scheme. Thus, moving from the deterministic scheme to one proposed here effectively means moving from a scheme limited by the photon collection efficiency to a scheme limited by spin coherence. If a hybrid of the HoS and HoD schemes is employed, the generation time falls somewhere between the curves for those schemes, with the fraction of photons generated via each method determining exactly where.

For the two proposed schemes there are additional factors that affect the fidelity that are not present in the deterministic scheme, including decoherence of the emitter and auxiliary spin(s) during the longer construction time and (for the HoS scheme) multiple photon pair production. Here we investigate the scaling of these sources of infidelity and compare them to the limits set by imperfect two-qubit spin-spin entangling gates, as well as the initial entanglement fidelities of the emitter photon and photon pair sources. We require one extra spin-spin

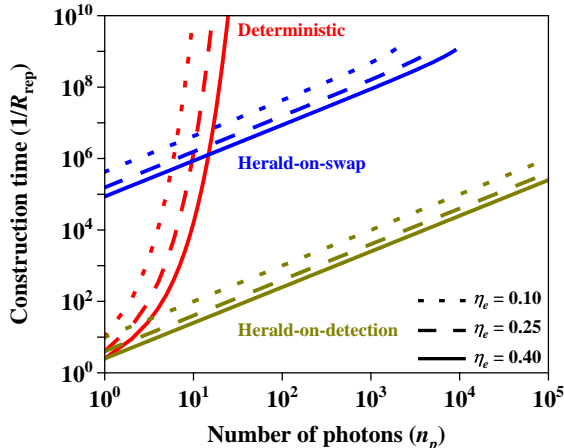


FIG. 3. Time to make photonic graph states of size n_p in units of the repetition period. The deterministic (red), HoS (blue), and HoD (yellow) schemes are compared. The three curves of each color represent emitter photon collection efficiencies $\eta_e \in \{0.1, 0.25, 0.4\}$. Polynomial scaling in the heralded schemes allows for the construction of larger graphs. Results are omitted where decoherence and false heralds bring the fidelity under 50% for reasonable experimental parameters. In the HoS scheme, fidelity can be sacrificed to improve the rate for the construction of small graph states if desired. A full description of these estimates is given in Appendix D.

entangling gate each time we add a photon to the graph, in addition to the gates required to make the desired final graph [37], which exponentially suppresses the fidelity of large photonic graph states if the gates are not perfect. Additionally, any infidelity of the photon pair source in the HoS scheme adds to the overall infidelity. Here, we demonstrate that if sufficient error correction or entanglement purification is possible [49], the additional sources of infidelity inherent to our scheme do not themselves prohibit exceedingly large graph states. For a full discussion of our experimental model and relevant sources of infidelity, see Appendix D.

In modeling decoherence under the usual dephasing map, any emitters or auxiliary spins will remain invariant with a probability $D(t, \tau) = \frac{1}{2}(1 + e^{-t/\tau})$, for the duration t until they are projectively measured. In either scheme, the emitter is reinitialized with each attempt to add a new photon to the larger graph, and hence the time it is required to remain coherent is reset. Furthermore, the classical conditioning offered by this “emit then add” method means the emitter is only required to remain coherent for the attempts where the relevant joint or single photon measurements are a success. Any auxiliary spins, on the other hand, are required to remain coherent for the duration of time they remain a part of the larger graph state in construction. The average time for the successful addition of a new photon to the larger graph goes as t_{rep}/P_s , where $t_{\text{rep}} = R_{\text{rep}}^{-1}$ is the repetition period of the excitation, and P_s is the probability of a successful

joint or single photon measurement for the HoS or HoD schemes, respectively. Note that in the HoD scheme we assume $P_s = \eta_e$. Hence, the total contribution to the final state fidelity from the emitter and any auxiliary spins is

$$F_D^{(e)}(n_p) = \left(\frac{1}{2} \left(1 + e^{-t_{\text{rep}}/\tau} \right) \right)^{n_p}, \quad (1a)$$

$$\langle F_D^{(s)}(n_p, P_s) \rangle = \frac{1}{2} \left(1 + e^{-n_p t_{\text{rep}}/P_s \tau} \right), \quad (1b)$$

where we include a superscript to denote emitter (e) and auxiliary spin (s) qubits, and we have used the same coherence time τ for the emitter and auxiliary spins in the system.

For the HoS scheme, we assume a standard SPDC source to generate the required entangled photon pairs [50]. The multi-pair emission of such a source introduces an additional infidelity in the entanglement swapping procedure. We denote P_t as the overall probability that a true Bell state is heralded and measured after constructing the graph. In general, $P_t < P_s$ due to false heralding. A primary source of false heralding is when the emitter photon is not collected but the SPDC source produces two or more photon pairs that lead to a detection pattern, falsely signaling a successful swap. False heralding due to two signal photons is a well known and ubiquitous problem in entanglement swapping with photon pair sources based on nonlinear optics [38]. We can write an expression for the fidelity of the entanglement swapping procedure, P_t/P_s , using the known statistical distribution of entangled photon pairs produced via SPDC. Here, we assume photon number-resolved detection and perfect collection and detection of the signal photon once produced. This is because loss on that channel can generally be minimal and primarily affects the rate rather than the swapping fidelity (see Appendix D for the full calculation, including further experimental factors not discussed here). Furthermore, the intention here is to show that even quite low efficiency collection of the emitter photon can allow the generation of graph states. The probability of producing two entangled photon pairs is proportional to the square of the probability of producing a single entangled pair, and is controllable via the pump power of the SPDC (parameterized here by the quantity ξ [38]), thus introducing a tradeoff between rate and fidelity. The fidelity, $F_{\text{swap}} = P_t/P_s$, is given by

$$P_t(\eta_e, \xi) = \eta_e(1 - \xi)^2\xi, \quad (2a)$$

$$P_s(\eta_e, \xi) = [\eta_e\xi + (1 - \eta_e)\xi^2] (1 - \xi)^2, \quad (2b)$$

$$F_{\text{swap}}(\eta_e, \xi) = \frac{\eta_e}{\eta_e + (1 - \eta_e)\xi}. \quad (2c)$$

In the absence of decoherence of the spins, we could simply work at $\xi \ll 1$ (very low pair generation rate) to reduce the false heralding and increase the overall fidelity. However, this slows the rate of the graph production and introduces infidelity due to decoherence of the auxiliary

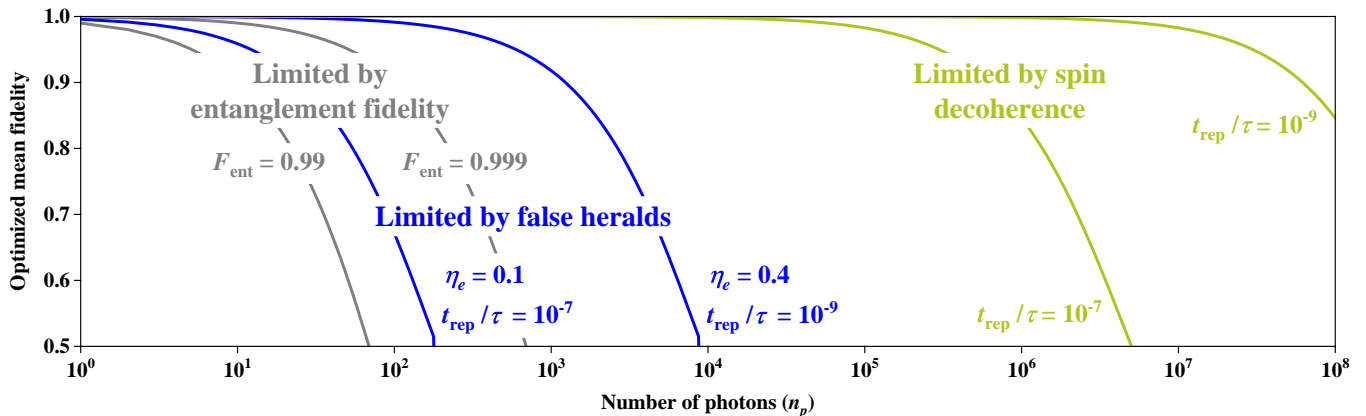


FIG. 4. Graph state fidelity versus photon number (n_p) for several different regimes of operations, and variable emitter-photon collection efficiencies (η_e) and dephasing timescales (t_{rep}/τ). Gate and pair generation fidelities (grey) exponentially preclude the construction of large graph states in any scheme utilizing our “emit then add” method. With sufficient error correction or purification around these fidelities, regimes limited by false heralds and decoherence (blue) and decoherence alone (yellow), allow for the construction of significantly larger graph states.

spin(s). Given a set of experimental parameters, the rate of pair production can be optimized by tuning ξ to maximize the overall fidelity of the desired graph state, balancing the infidelity due to false heralds against the decoherence.

We present a simple example comparing these additional sources of infidelity to the limits set by spin-spin entangling gates and initial entanglement fidelities, for the case of constructing a graph state on a single auxiliary spin. Figure 4 depicts these estimates over a few regimes. The combined effect of false heralds and decoherence (blue) set the fidelity as

$$F(n_p, \eta_e, \xi) = F_{\text{swap}}(\eta_e, \xi)^{n_p} F_D^{(e)}(n_p) \times \langle F_D^{(s)}(n_p, P_s(\eta_e, \xi)) \rangle, \quad (3)$$

which we optimize over ξ , for fixed n_p and η_e . When only limited by decoherence (yellow), we can employ Equation (3), except now fixing $F_{\text{swap}}(\eta_e, \xi) = 1$ and removing the need to optimize the fidelity. These estimates are applicable when constructing large star graph states—the local-unitary equivalent to a Greenberger-Horne-Zeilinger (GHZ) state—and 1D cluster states.

V. REALIZING SECURE TWO-PARTY COMPUTATION

As one application of our HoD scheme, we describe a method for securely computing an arbitrary Boolean function $f : \{0, 1\}^{\times n} \rightarrow \{0, 1\}$ of either two parties or a restricted class of multi-party functions. As a special type of MBQC, our protocol, \mathcal{P} , performs the calculation through a sequence of measurements on distributed graph states. Only Pauli measurements are needed, so \mathcal{P} can be implemented using HoD and the generation of the requisite resource state happens in parallel with

the computation without any need for photonic memory. Furthermore, the size of each graph state required for \mathcal{P} is fixed at 12 photons, regardless of the number of parties or the size of their inputs, which should be possible with high fidelity on current state-of-the-art hardware.

Secure multi-party computation (MPC) is a task in which two or more parties compute some function on their individually held variables without revealing the values of the variables to each other [51, 52]. For example, in Yao’s famous millionaire problem, two parties want to determine whose bank account has the most money without actually revealing how much money is in each account. MPC is a deeply-studied topic in both classical and quantum cryptography, and a variety of MPC protocols have been proposed achieving different levels of security and relying on different operational assumptions [53].

We propose an unconditionally secure method for restricted MPC that includes all two-party computations and requires only two rounds of public communication regardless of the size of the computational input. Our scheme follows a well-known approach of decomposing an MPC into “offline” and “online” phases [54–56]. In the offline phase, some universal computational resource is distributed to all the parties. Crucially, this resource does not depend on the particular function being computed other than its input size. Then in the online phase this resource is used to compute some chosen function of the parties’ inputs. For example, in the classical setting one well-known computational resource is a special form of shared randomness known as “Beaver triples,” which can be used to efficiently compute logical AND gates in the online phase [57]. The problem of MPC then reduces to secure and efficient methods for distributing Beaver triples in the offline phase. In a similar spirit, our protocol involves distributing certain quantum graph states in the offline phase which then enable the computation

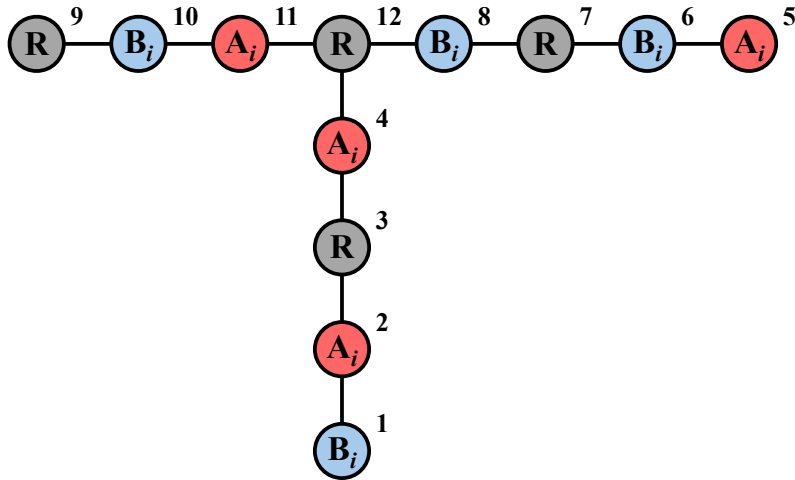


FIG. 5. For each requisite bit conjunction in Stage I, the 12-qubit graph state $|G\rangle$ is distributed to **R** (the Referee) and pair of parties labeled **A_i** (Alice), **B_i** (Bob). When the measurement sequence detailed by the protocol is implemented honestly a correlation is generated between the parties, such that $a_i b_i = m_{i,12} + \alpha_i + \beta_i$, where α_i and β_i are locally computed by Alice and Bob, respectively, from openings made in Stage II. Hence, we utilize each copy of the state to achieve a homomorphic encryption of a bit conjunction $a_i b_i$, where Alice, Bob, and the Referee each possess an additive share. The numeric script above each qubit reflects an example photon emission order for the generation of the graph state.

of a logical AND in the online phase, through quantum measurement and classical post-processing. Beyond its relatively low communication costs, a significant advantage of our protocol is that the parties can, in principle, use self-testing methods to verify that some untrusted Source is faithfully distributing the correct graph state [58, 59], an ability that does not exist for classical shared randomness.

Suppose that N parties $\mathbf{P}_1, \dots, \mathbf{P}_N$ wish to compute some Boolean function $f(\mathbf{x}_1, \dots, \mathbf{x}_N)$, where \mathbf{x}_k is a string of bits representing the input for party \mathbf{P}_k . In addition to correctness, the evaluation of f should be done securely such that the parties learn no more information about the individual $\mathbf{x}_1, \dots, \mathbf{x}_N$ beyond their own input and what is revealed in the function value $f(\mathbf{x}_1, \dots, \mathbf{x}_N)$. To achieve this task, we propose a method of delegated computation in which a non-collaborating Referee, **R**, is introduced to assist in the computation of $f(\mathbf{x}_1, \dots, \mathbf{x}_N)$. To maintain privacy, **R** also should not learn any more information about the \mathbf{x}_k beyond what is implied by the computed value $f(\mathbf{x}_1, \dots, \mathbf{x}_N)$, nor does **R** reveal any more information to the other parties, other than what is necessary to evaluate f securely.

We utilize the fact that every Boolean function f can be expressed in an algebraic normal form (ANF), which presents f as a sum (mod 2) of different variable conjunctions. That is, we can write $f = \sum_{i=1}^{\mathfrak{R}} c_i$, where each c_i is the logical AND of a certain group of input variables. By combining variables belonging to the same party, every c_i becomes the conjunction of at most N variables, each one belonging to a different party. In this work, we restrict attention to functions f that admit an ANF whose conjunctions involve no more than two variables.

This covers the entire class of two-party functions, but also includes certain multi-party functions, such as the three-party majority function $\varphi_3(x, y, z) = xy + xz + yz \pmod{2}$, which outputs the majority value among inputs $x, y, z \in \{0, 1\}$. In general, the functions we consider have the form $f = \sum_{i=1}^{\mathfrak{R}} a_i b_i + \sum_{k=1}^N z_k$, where a_i and b_i are the inputs bits of each quadratic conjunction, belonging to different parties, and z_k is the input bit of the linear part of f , belonging to party \mathbf{P}_k . We let $\tilde{\mathbf{x}}_k \subset \{a_i, b_i, z_k\}_{i=1, k=1}^{\mathfrak{R}, N}$ denote all the inputs of f belonging to \mathbf{P}_k . Furthermore, if each $\tilde{\mathbf{x}}_k$ is no more than M bits, then $\mathfrak{R} \leq \binom{N}{2} (M-1)^2$.

The offline phase of \mathcal{P} calls for the distribution of \mathfrak{R} copies of the graph state $|G\rangle$ depicted in Figure 5, one copy for each conjunction $a_i b_i$ in f . The generation of each copy of $|G\rangle$ requires only two auxiliary spins in either of the experimental schemes we propose [37]. We denote the i^{th} copy as $|G_i\rangle$, and their distribution can be conducted in parallel. The specific qubits in each $|G_i\rangle$ are given to the parties $\{\mathbf{A}_i, \mathbf{B}_i\} \subset \{\mathbf{P}_1, \dots, \mathbf{P}_N\}$ who, respectively, have inputs $\{a_i, b_i\}$ to the conjunction $a_i b_i$. We assume without loss of generality that each party receives qubits belonging to at least one $|G_i\rangle$, an assumption that can be trivially ensured by adding conjunctions to f of inputs that are identically zero. This is a technical requirement of our protocol since the $|G_i\rangle$ will ultimately be used to generate one-time pad bits, and each party needs at least one. In practice, the $|G_i\rangle$ can be generated by an untrusted quantum Source, and their correctness can be certified using self-testing methods (see Appendix B3). Specific steps for building $|G\rangle$ using a quantum emitter are presented in Appendix C2.

The online phase of \mathcal{P} thereafter is split into two stages.

Stage I involves measuring Pauli observables, X, Y, Z , on \mathfrak{R} copies of the graph state $|G\rangle$, depicted in Figure 5, following the sequence below.

Stage I: Obtaining correlations from quantum states.

Input: For $i \in \{1, \dots, \mathfrak{R}\}$ a copy of $|G_i\rangle$ is distributed by the Source to \mathbf{R} (the Referee) and pair of parties \mathbf{A}_i (Alice) and \mathbf{B}_i (Bob). The following measurement sequence is performed by $\{\mathbf{A}_i, \mathbf{B}_i\} \subset \{\mathbf{P}_1, \dots, \mathbf{P}_N\}$ who holds inputs $\{a_i, b_i\}$, respectively.

- (I.1). \mathbf{B}_i and \mathbf{A}_i measure Z on qubits 1 and 5, respectively, obtaining measurement outcomes $m_{i,1}$ and $m_{i,5}$.
- (I.2). $\mathbf{A}_i, \mathbf{B}_i$, and \mathbf{R} measure X on qubits 2, 6, and 9, respectively, obtaining measurement outcomes $m_{i,2}$, $m_{i,6}$, and $m_{i,9}$.
- (I.3). \mathbf{R} measures Z on qubits 3 and 7, and \mathbf{B}_i likewise measures Z on qubit 10. They obtain measurement outcomes $m_{i,3}$, $m_{i,7}$, and $m_{i,10}$.
- (I.4). \mathbf{A}_i applies $Z^{m_{i,2}}$ to qubit 4 and measures $W^{a_i} Z (W^\dagger)^{a_i}$ on qubits 4 and 11 thereafter, where $W \equiv (iX)^{1/2}$. She obtains measurement outcomes $m_{i,4}$ and $m_{i,11}$. Note that $WZW^\dagger = Y$.
- (I.5). \mathbf{B}_i applies $Z^{m_{i,6}}$ to qubit 8 and measures $W^{m_{i,10}} Z (W^\dagger)^{m_{i,10}}$ thereafter, obtaining measurement outcome $m_{i,8}$.
- (I.6). \mathbf{R} measures $V^{m_{i,9}} X (V^\dagger)^{m_{i,9}}$ on qubit 12, where $V \equiv (-iZ)^{1/2}$, obtaining measurement outcome $m_{i,12}$. Note that $VXV^\dagger = Y$.

When all the measurements through step (I.3) are made as specified, the parties obtain correlated measurement outcomes satisfying the relationships

$$m_{i,1} + m_{i,2} + m_{i,3} = 0, \quad (4a)$$

$$m_{i,5} + m_{i,6} + m_{i,7} = 0, \quad (4b)$$

$$m_{i,9} + m_{i,10} = 0, \quad (s_i \equiv m_{i,9} = m_{i,10}). \quad (4c)$$

When the subsequent measurements through step (I.6) are made as specified, the Referee's final outcome satisfies

$$a_i b_i = m_{i,12} + \alpha_i + \beta_i, \quad (5)$$

where

$$\alpha_i = a_i(m_{i,1} + b_i + 1) + (m_{i,4} + m_{i,11}) \quad (6a)$$

$$\beta_i = (m_{i,5} + a_i)b_i + m_{i,8}. \quad (6b)$$

The end result of each iteration i of the measurement sequence leaves Alice, Bob, and the Referee with additive homomorphic shares of the bit conjunction $a_i b_i$. The only temporal restrictions on the sequence, are that measurements in steps (I.1)-(I.3) need be performed prior to

those in steps (I.4)-(I.6). Furthermore, we can understand both α_i and β_i as two layers of data that are nest together by one-time pads. For α_i , the bit $(m_{i,4} + m_{i,11})$ serves as a pad (known only to Alice) for the two multipliers a_i and $(m_{i,1} + b_i + 1)$; while within the latter multiplier, the bit $m_{i,1}$ serves as a pad (known only to Bob) for $b_i + 1$. A similar interpretation holds for β_i .

The padded structure of the bit values obtained in Stage I enables the calculation of each α_i and β_i using public communication (i.e. "openings") and local processing in Stage II of \mathcal{P} , without revealing any information about the corresponding a_i or b_i . A second round of communication thereafter opens only the collective sum $\sum_{i=1}^{\mathfrak{R}} a_i b_i$ of the bit conjunctions encrypted in Stage I, while also adding the linear term $\sum_{k=1}^N z_k$, thereby allowing the secure evaluation of f .

Stage II: Public communication and classical post-processing.

Input: Let $\mathcal{A}_k \subset \{1, \dots, \mathfrak{R}\}$ denote the set of conjunctions in which \mathbf{P}_k played the role of \mathbf{A}_i , and similarly, let $\mathcal{B}_k \subset \{1, \dots, \mathfrak{R}\}$ denote the set of conjunctions in which \mathbf{P}_k played the role of \mathbf{B}_i . \mathbf{P}_k inputs their bits from $\{\alpha_i\}_{i \in \mathcal{A}_k}$ and $\{\beta_i\}_{i \in \mathcal{B}_k}$, along with their bit z_k . \mathbf{R} inputs their bits from $\{m_{i,12}\}_{i=1}^{\mathfrak{R}}$.

- (II.1). For each $i \in \{1, \dots, \mathfrak{R}\}$,
 - (a). \mathbf{A}_i opens $c_{i,A} \equiv m_{i,5} + a_i$ and \mathbf{B}_i opens $c_{i,B} \equiv m_{i,1} + b_i + 1$.
 - (b). \mathbf{A}_i locally computes $\alpha_i = c_{i,B} a_i + (m_{i,4} + m_{i,11})$ and \mathbf{B}_i locally computes $\beta_i = c_{i,A} m_{i,10} + m_{i,8}$.
- (II.2). For each $k \in \{1, \dots, N\}$, \mathbf{P}_k opens $\Gamma_k \equiv z_k + \sum_{i \in \mathcal{A}_k} \alpha_i + \sum_{i \in \mathcal{B}_k} \beta_i$. Concurrently, \mathbf{R} opens $\Gamma_{\mathbf{R}} \equiv \sum_{i=1}^{\mathfrak{R}} m_{i,12}$.
- (II.3). All the parties locally compute $f = \Gamma_{\mathbf{R}} + \sum_{k=1}^N \Gamma_k$.

It should be noted that by parallelization, Stage II can be performed using just two rounds of simultaneous communication between the parties. Indeed, each \mathbf{P}_k needs to broadcast at most two public messages, the first being no more than $\log \mathfrak{R}_1$ bits, and the second being just one bit. When run in parallel, all the step (II.1) messages can be broadcast concurrently, and likewise for the step (II.2) messages. Moreover, this classical communication can be done after all quantum measurements are performed since the choice of local measurement at each step in \mathcal{P} does not depend on the classical message of any other party. Experimentally this is very desirable since it means that \mathcal{P} can be implemented in three parts: (i) entanglement distribution (offline phase), (ii) local measurement of qubits (online phase Stage I), and (iii) classical post-processing (online phase Stage II). Without the use of quantum memory it is not possible to cleanly separate parts (i) and (ii), and in practice each state $|G_i\rangle$ can

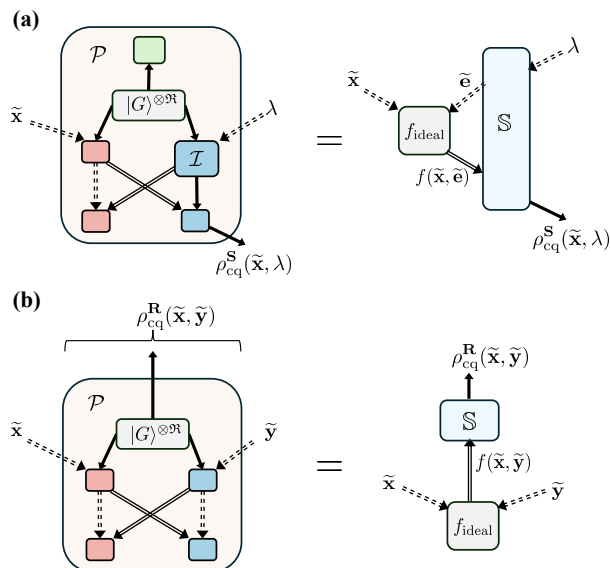


FIG. 6. Malicious attacks on \mathcal{P} by \mathbf{S} and \mathbf{R} . (a) General attack by \mathbf{S} . The attack is described by a quantum instrument \mathcal{I} that acts on the qubits of $|G\rangle^{\otimes R}$ distributed to \mathbf{S} , with possible dependence on some side-information λ . For every $\tilde{\mathbf{x}}$ of \mathbf{P} , the attack will generate for \mathbf{S} a classical-quantum state $\rho_{\text{cq}}^{\mathbf{S}}(\tilde{\mathbf{x}}, \lambda)$ that depends on all public communication in the protocol. We show there exists a simulator \mathbb{S} in place of party \mathbf{S} in the ideal world that submits some input $\tilde{\mathbf{e}}$ to f_{ideal} and then uses the output $f(\tilde{\mathbf{x}}, \tilde{\mathbf{e}})$ to generate the same $\rho_{\text{cq}}^{\mathbf{S}}(\tilde{\mathbf{x}}, \lambda)$ achieved in the real world. (b) General attack by \mathbf{R} . We again show there exists a simulator \mathbb{S} that takes the places of \mathbf{R} in the ideal world, receiving just the function output $f(\tilde{\mathbf{x}}, \tilde{\mathbf{y}})$ and outputting the classical-quantum state $\rho_{\text{cq}}^{\mathbf{R}}(\tilde{\mathbf{x}}, \tilde{\mathbf{y}})$ achieved in the real world, as shown to the right.

be measured in a streaming manner. This type of implementation does not affect the performance or security of the protocol.

Security. We now turn to analyze the security of \mathcal{P} . At a high level, our security claim is that if \mathbf{R} plays honestly, then \mathcal{P} reveals no more information about $\tilde{\mathbf{x}}_k$ of an honest party \mathbf{P}_k , beyond what can be inferred from the function values $f(\tilde{\mathbf{x}}_1, \dots, \tilde{\mathbf{x}}_N)$. Here, an honest party is anyone who executes the steps of \mathcal{P} faithfully. Our protocol also offers some security against a cheating \mathbf{R} . Namely, if all N parties follow \mathcal{P} honestly, then \mathbf{R} is also unable to infer any information about the inputs beyond what can be computed from $f(\tilde{\mathbf{x}}_1, \dots, \tilde{\mathbf{x}}_N)$.

Note that for N parties $\mathbf{P}_1, \dots, \mathbf{P}_N$ these claims allow for the possibility that any subset of $N - 1$ parties are colluding against a single party. The colluding parties are allowed to share an unlimited amount of classical and quantum communication over side channels, and they can thus collectively be viewed as a single party \mathbf{S} . In this case, the task essentially reduces to a problem between the two parties \mathbf{P} and \mathbf{S} , and \mathbf{R} . We let $\tilde{\mathbf{x}}$ denote the input of \mathbf{P} and $\tilde{\mathbf{y}}$ as the total input of all the colluding parties constituting \mathbf{S} . The goal, then, is to securely compute

$f(\tilde{\mathbf{x}}, \tilde{\mathbf{y}})$.

In this work we adopt a simulation based notion of security. Consider first an ideal world in which there exists some device f_{ideal} that privately receives inputs $\tilde{\mathbf{x}}$ and $\tilde{\mathbf{y}}$ from \mathbf{P} and \mathbf{S} , respectively, and then outputs $f(\tilde{\mathbf{x}}, \tilde{\mathbf{y}})$ to \mathbf{P} , \mathbf{S} , and \mathbf{R} . These two worlds are described more thoroughly in Appendix B 1. Intuitively, we want the ideal world to reveal at least as much information about the inputs $(\tilde{\mathbf{x}}, \tilde{\mathbf{y}})$ than what is revealed to any dishonest party acting maliciously in the real world.

This intuition is made precise through the notion of a simulator. A simulator, \mathbb{S} , in this setting is some device that can take the place of a party $\mathbf{X} \in \{\mathbf{P}, \mathbf{S}, \mathbf{R}\}$ and interact with the ideal functionality f_{ideal} from the viewpoint of party \mathbf{X} . Consider now any action taken by a potentially dishonest party in \mathcal{P} . Our security definition is that there must exist a simulator \mathbb{S} interacting with f_{ideal} that exactly reproduces what the dishonest party obtains from \mathcal{P} . This operationally captures the idea that the adversary learns no more information about an honest party's input, other than what can be inferred directly from an ideal evaluation of f . Figure 6 depicts the two forms of malicious attacks for which we prove that \mathcal{P} is secure. A formal security definition and full proof are provided in Appendix B 1.

Performance. To handle experimental errors in the above protocol, we can employ a simple repetition code to suppress the effects of any infidelity in our ability to make each copy of $|G\rangle$ in the offline phase of \mathcal{P} . By determining the total bit error probability associated with each share of $a_i b_i$, an arbitrarily small total bit error probability ϵ_f on the output f can be chosen to set the number of repetitions required for Stage I. We use this information to estimate the lower bound rate of computation at which N parties can compute f on their M -bit inputs. Details are provided in Appendix B 2.

Functionally, our protocol allows for the secure implementation of any two-party Boolean function, f , by repeatedly generating and distributing copies of the 12-qubit state $|G\rangle$. The number of required copies depends (polynomially) on the size of the input, M , and the desired final error probability, ϵ_f . A pair of auxiliary spins can be employed to generate each copy constructed in parallel, and additional emitters can be employed to speed up the construction. Furthermore, these spins need only remain coherent for at most the time to make each copy of $|G\rangle$, a requirement easily met with current trapped ion or atom array systems. Using the fidelity estimates established in Section IV and detailed in Appendix D, we can conservatively estimate the maximum possible bit error probability associated with each copy from the complement of the probability that no bit error occurs, that is, the complement of the fidelity to produce $|G\rangle$ in our proposed HoD scheme. In Figure 7, we plot the lower bound rate of computation at which our protocol can operate with error correction, in units of R_{rep} , against the size of each party's input, M , for total acceptable error probabilities $\epsilon_f = \{10^{-3}, 10^{-12}\}$.

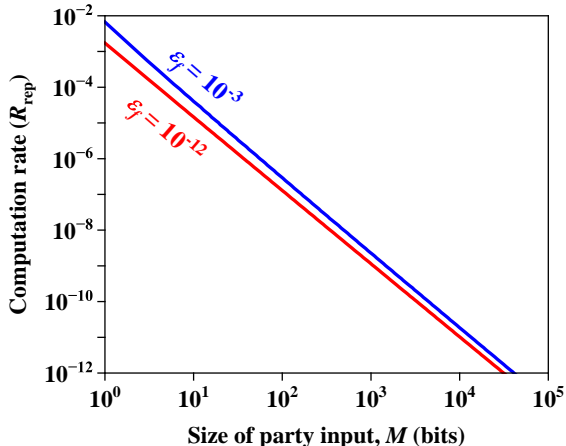


FIG. 7. Error corrected two-party computation rate versus the number of requiring conjunctions in f using the HoD scheme, shown for two acceptable error probabilities on the computation (ϵ_f). The rate is expressed in units of the repetition rate of excitation of the chosen quantum emitter, R_{rep} , which can be in the range of $10^6 - 10^9 \text{ s}^{-1}$ for highly coherent emitters. The individual bit error probabilities for each copy of $|G\rangle$ is 0.012, assuming $\eta_e = 0.4$, $F_{\text{ent}} = 0.999$, and $t_{\text{rep}}/\tau = 10^{-9}$ (see. Appendix D for details). We see that these parameters allow virtually unlimited reduction in the total error probability with minimal change in the overall rate.

We assume that M here is the number of bits each party needs to perform a conjunction on, neglecting the single linear bit they each input as well.

VI. DISCUSSION AND CONCLUSION

The schemes introduced here naturally lend themselves to various extensions and modifications to increase functionality. First, combining with a high degree of multiplexing, such as between many arrays of atoms or ions, would increase the generation rate with a linear factor in the degree of multiplexing. Incorporating this with heralding means that photons can be routed upon suc-

cessful generation of spin-photon entanglement. Another extension is the opportunity for substantial spectral engineering of the idler photon in the HoS scheme. As mentioned above, the idler photon can be produced at virtually any arbitrary wavelength regardless of the emission wavelength of the emitting spin, including using a superconducting qubit as the spin and generating a signal-idler pair with a microwave signal and an optical idler [60]. We also point out that the bandwidth of the idler photon can be different than the typically narrow and fixed bandwidth of the emitter. Filtering, time lensing [61], and/or source engineering [27, 62] can enable substantial broadening or narrowing of the idler photon compared to the emitter photon.

In this work, we have demonstrated the feasibility of generating photonic graph states with inefficient quantum emitters and give a central example of its applications to secure multi-party computation. Significantly, our schemes offer polynomial scaling in the time to construct graph states of hundreds of photons with high fidelity on current generation trapped ion experiments [14, 15], even when the collection efficiency of emitter photons is poor. The “emit then add” approach requires additional resource costs for making graph states, but we show that it is feasible with current and near-term experimental hardware. Our scheme is a toolbox for making large entangled photonic states for MBQC and other applications that are limited by spin decoherence rather than photon collection efficiency. We specifically show an application to realize distributed multi-party computation that is feasible in the near-term with current hardware.

ACKNOWLEDGMENTS

We acknowledge helpful discussions with Kejie Fang and Vito Scarola. E.C. thanks Christian Schaffner and Ian George for some helpful explanations on multi-party computation and security. This work was supported by the NSF Quantum Leap Challenge Institute on Hybrid Quantum Architectures and Networks (NSF Award No. 2016136).

Appendix A: Preliminaries on graph states

For an arbitrary graph $G = (V, E)$ with vertices $V = \{a_1, \dots, a_n\}$ and edge set $E \subset V \times V$, consider the n -qubit operator obtained by performing a controlled- Z gate, $CZ_{a,b}$, between every $(a, b) \in E$. We denote this global operator by

$$U_G = \prod_{(a,b) \in E} CZ_{a,b}. \quad (\text{A1})$$

The graph state associated with the graph G is the n -qubit state

$$|G\rangle = U_G |+\rangle^{\otimes n}. \quad (\text{A2})$$

Note that $|+\rangle^{\otimes n}$ is stabilized by n commuting operators $\{X_a\}_{a \in V}$. Hence the stabilizer of $|G\rangle$ can be understood by examining the how the X_a transform under U_G . Since $CZ_{a,b}(X_a)CZ_{a,b} = X_a Z_b$, it follows that the stabilizer of $|G\rangle$ is generated by the operators $\{K_a\}_{a \in V}$, where

$$\begin{aligned} K_a &= U_G X_a U_G \\ &= X_a \prod_{b \in N_a} Z_b \\ &= X_a \prod_{b \in V} Z_b^{\Gamma_{a,b}} \quad \forall a \in V, \end{aligned} \quad (\text{A3})$$

and Γ is the adjacency matrix of G .

For any n -qubit graph state $|G\rangle$, we can generate an orthonormal basis for \mathbb{C}_2^N , called the associated graph basis. The basis vectors have the form

$$Z^{\mathbf{r}} |G\rangle \quad \text{where} \quad Z^{\mathbf{r}} := Z_1^{r_1} \otimes Z_2^{r_2} \otimes \cdots \otimes Z_N^{r_N}, \quad (\text{A4})$$

and we will call $\mathbf{r} = (r_1, r_2, \dots, r_n) \in \mathbb{Z}_2^n$ a conditional phase vector and each bit r_k *phase information* for qubit k . To see that these states are orthogonal, let \mathbf{r} and \mathbf{r}' be two distinct conditional phase vectors, and suppose their bit values differ in position a . Then K_a will anti-commute with $Z^{\mathbf{r}} Z^{\mathbf{r}'}$, and so

$$\langle G | Z^{\mathbf{r}} Z^{\mathbf{r}'} |G\rangle = \langle G | Z^{\mathbf{r}} Z^{\mathbf{r}'} K_a |G\rangle = -\langle G | K_a Z^{\mathbf{r}} Z^{\mathbf{r}'} |G\rangle = -\langle G | Z^{\mathbf{r}} Z^{\mathbf{r}'} |G\rangle. \quad (\text{A5})$$

We will be particularly interested in how the graph basis states transform under the local Pauli measurements of Y and Z . For a binary vector $\mathbf{r} \in \mathbb{Z}_2^n$ and subset of nodes $S \subset V$, let $\mathbf{r} - S$ denote the vector of length $n - |S|$ obtained from \mathbf{r} by removing the coordinates in S . Suppose that for an initial graph basis state $Z^{\mathbf{r}} |G\rangle$, either Y or Z is measured on qubit a and outcome $m_a \in \{0, 1\}$ is received. The initial state transforms as follows:

$$Z_a : \quad Z^{\mathbf{r}} |G\rangle \mapsto \left(\prod_{b \in N_a} Z_b^{m_a} \right) Z^{\mathbf{r}-a} |G - a\rangle, \quad (\text{A6a})$$

$$Y_a : \quad Z^{\mathbf{r}} |G\rangle \mapsto \left(\prod_{b \in N_a} (-iZ_b)^{1/2} Z_b^{r_a + m_a} \right) Z^{\mathbf{r}-a} |\tau_a(G) - a\rangle, \quad (\text{A6b})$$

where $\tau_a(G)$ is the local complementation of G at vertex a , i.e. $\tau_a(G)$ is the graph $(V, E\Delta E(N_a, N_a))$, and $\tau_a(G) - a$ is the graph obtained by removing a from $\tau_a(G)$ [63]. Explicitly,

$$|\tau_a(G)\rangle = (-iX_a)^{1/2} \left(\prod_{b \in N_a} (iZ_b)^{1/2} \right) |G\rangle, \quad (\text{A7})$$

describes a set of single-qubit rotations comprising a local complementation. Note that the Y_a post-measurement state can always be transformed back to the associated graph basis by performing $(iZ_b)^{1/2}$ on each $b \in N_a$. For the special case of measurement at a leaf in the graph, a vertex with only a single neighbor such that $\tau_a(G) = G$, the Y_a post-measurement state after rotation back to the graph basis is effectively a Z_a post-measurement state up to the conditional phase flip $Z_b^{r_a}$.

1. Phase transmission along a chain

Consider the effect of locally measuring along some linear chain in graph G . Let $a_1, a_2, a_3, \dots, a_n, a_{n+1}$ denote the constituent qubits, with a_1 being the first node in the chain and a_{n+1} being the final node, which is connected to the remainder of the graph and left unmeasured in this sub-routine. The specific measurement sequence consists of measuring Y on a_1 and $(-iZ)^{1/2} Y (iZ)^{1/2} = -X$ on a_k for all $k = 2, \dots, n-1$. If the total state prior to measurement is a graph basis state $Z^{\mathbf{r}} |G\rangle$ and $(m_{a_1}, \dots, m_{a_{n-1}})$ is the binary sequence of outcomes from these measurements, then by Equation (A6b) the overall state evolution is

$$Y_{a_1}, (-X_{a_2}), \dots, (-X_{a_{n-1}}) : \quad Z^{\mathbf{r}} |G\rangle \mapsto [-iZ_{a_n}]^{1/2} Z_{a_n}^{\Omega} Z^{\mathbf{r}-\{a_1, \dots, a_{n-1}\}} |G - \{a_1, \dots, a_{n-1}\}\rangle, \quad (\text{A8})$$

where $\Omega = \sum_{i=1}^{n-1} (r_{a_i} + m_{a_i}) \bmod 2$. Crucially, each m_{a_k} is a random bit uncorrelated from \mathbf{r} and any other measurement data. Hence, we can think of each m_{a_k} as a one-time pad that is added to the conditional phase information r_{a_k} when passing from node a_k to a_{k+1} .

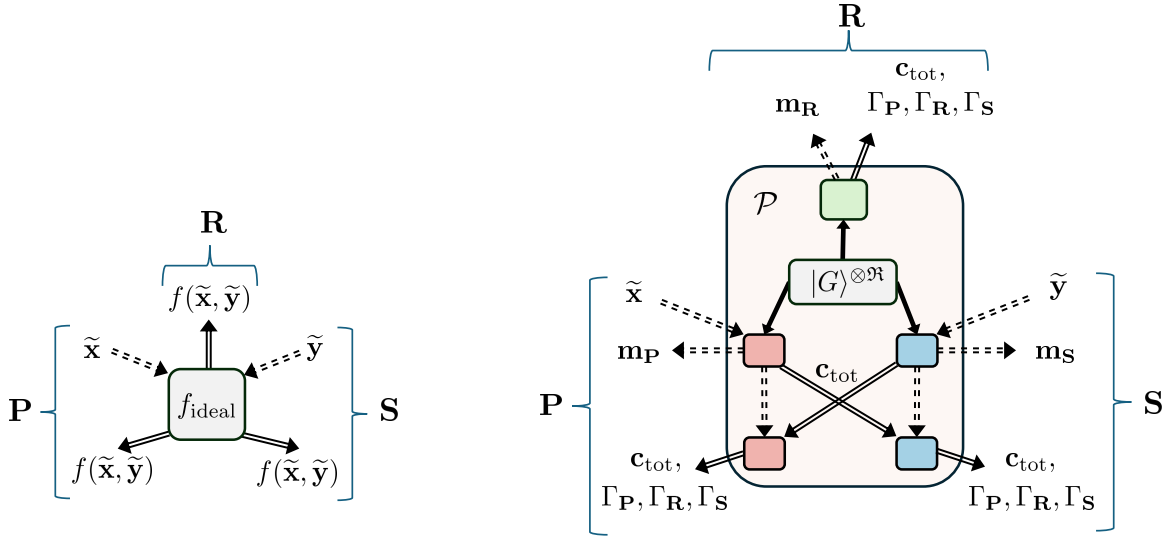


FIG. 8. Diagram of the security setting for \mathcal{P} , as described in Section V. An ideal device (left) publicly broadcasts the function value $f(\tilde{\mathbf{x}}, \tilde{\mathbf{y}})$ for private inputs $(\tilde{\mathbf{x}}, \tilde{\mathbf{y}})$. A high-level depiction of \mathcal{P} (right), with $\mathbf{m}_{\mathbf{X}}$ denoting the collective local measurement outcomes for party $\mathbf{X} \in \{\mathbf{P}, \mathbf{S}, \mathbf{R}\}$ and \mathbf{c}_{tot} denoting all the public communication in the first part of Stage II. The boxes (red, blue, green) indicate local processing by a given party ($\mathbf{P}, \mathbf{S}, \mathbf{R}$). Solid (dashed) double lines indicate public (private) classical information. Solid single lines indicate distributed quantum information.

2. Phase transmission at a fork

Consider the effect of measuring two qubits, a and b , that are connected to a single common node c . Suppose the total state prior to measurement is a graph basis state $Z^{\mathbf{r}}|G\rangle$. If m_a and m_b denote the binary outcomes when either Y or Z is measured on both qubits, the respective state transformations are given by

$$Y_a, Y_b : Z^{\mathbf{r}}|G\rangle \mapsto Z_c^{r_a+r_b+1} Z_c^{m_a+m_b} Z^{\mathbf{r}-\{a,b\}}|G-\{a,b\}\rangle, \quad (\text{A9a})$$

$$Z_a, Z_b : Z^{\mathbf{r}}|G\rangle \mapsto Z_c^{m_a+m_b} Z^{\mathbf{r}-\{a,b\}}|G-\{a,b\}\rangle, \quad (\text{A9b})$$

up to an overall phase. Hence, the key difference between the two measurements is that Y_a, Y_b transfers the conditional phase flip $Z_c^{r_a+r_b+1}$ onto the state $|G-\{a,b\}\rangle$ while Z_a, Z_b does not.

Appendix B: Secure multi-party computation

We prove the security of our multi-party computation protocol detailed in Section V via a simulation based argument, using the preliminaries of Appendix A. The measurement sequence described in Stage I along with the classical post-processing of Stage II together accomplish the computation of any Boolean function up to quadratic order in the parties' inputs. We verify this by tracing through the transformation of the graph state $|G\rangle$ (see Figure 5) in the stabilizer formalism, demonstrating the information that is transmitted along the graph in the form of phase flips conditioned on both the parties' inputs and their measurements. We establish security by demonstrating that the classically communicated information in the protocol reveals no new information to any of the other parties about their input, other than what they would learn from the final output of the computation. Subsequently, we detail how classical error correction can be utilized to suppress a bit error on the output of the computation. Finally, we discuss how self-testing can be employed to further secure against a possibly corrupt Source.

1. Security

We return to the security of our protocol \mathcal{P} , introduced in Section V, and present a formal proof. We adopt a simulation based notion of security, in which we present an idealized evaluation of f that receives inputs privately and returns only the correct function evaluation. Figure 8 depicts this security setting in both the ideal and real worlds. We show that all the classical and quantum information held by an adversary in any attack on the real protocol \mathcal{P}

can equivalently be simulated from the ideal evaluation of f . Hence all the information an adversary extracts about an honest party's input through \mathcal{P} is already accessible through an ideal evaluation of f . In this paper we address two forms of malicious attacks, depicted in Figure 6, where we assume without loss of generality that \mathbf{P} is the party playing honestly.

We begin by formalizing our security definition in the settings that follow. To clarify further, first consider when \mathbf{S} potentially deviates from the protocol. The most general physical action can be formally described by a quantum instrument \mathcal{I} that might depend on some classical side information λ [64]. For every $\tilde{\mathbf{x}}$ of \mathbf{P} , the instrument will generate for \mathbf{S} a classical-quantum (cq) state $\rho_{\text{cq}}^{\mathbf{S}}(\tilde{\mathbf{x}}, \lambda)$, which contains all of \mathbf{S} 's quantum registers along with classical registers recording all of the public communication $(\mathbf{c}_{\text{tot}}, \Gamma_{\mathbf{P}}, \Gamma_{\mathbf{S}}, \Gamma_{\mathbf{R}})$. To maintain consistency with the protocol, we assume \mathbf{S} still broadcasts some classical message when called for in the honest protocol, although this message can be generated in an arbitrary way. On the other hand, consider a case when \mathbf{R} deviates from the instruction of \mathcal{P} . Whenever \mathbf{P} and \mathbf{S} follow the protocol honestly on any pair of inputs $(\tilde{\mathbf{x}}, \tilde{\mathbf{y}})$, they will generate for \mathbf{R} the cq state $\rho_{\text{cq}}^{\mathbf{R}}(\tilde{\mathbf{x}}, \tilde{\mathbf{y}})$, from which any operation could be performed by \mathbf{R} to extract information.

Theorem 1. *For any two-party function $f(\tilde{\mathbf{x}}, \tilde{\mathbf{y}}) = z_{\mathbf{P}} + z_{\mathbf{S}} + \sum_{i=1}^{\mathfrak{R}} a_i b_i$, the protocol \mathcal{P} satisfies the following security conditions.*

1. (Correctness.) *If all the parties are honest, then for every input $(\tilde{\mathbf{x}}, \tilde{\mathbf{y}})$ the output of the ideal protocol can be locally computed from the outputs of \mathcal{P} .*

$$f(\tilde{\mathbf{x}}, \tilde{\mathbf{y}}) = \Gamma_{\mathbf{P}} + \Gamma_{\mathbf{S}} + \Gamma_{\mathbf{R}} \quad (\text{B1})$$

2. (Secure if only \mathbf{S} cheats.) *Suppose \mathbf{P} and \mathbf{R} follow \mathcal{P} honestly, but \mathbf{S} potentially deviates. Let $\rho_{\text{cq}}^{\mathbf{S}}(\tilde{\mathbf{x}}, \lambda)$ denote the total cq state held by \mathbf{S} at the end of \mathcal{P} , given input $\tilde{\mathbf{x}}$ of \mathbf{P} and side information λ . Then, there exists a simulator \mathbb{S} for \mathbf{S} interacting with the ideal functionality f_{ideal} that exactly reproduces $\rho_{\text{cq}}^{\mathbf{S}}(\tilde{\mathbf{x}}, \lambda)$ for all $\tilde{\mathbf{x}}$ and λ .*
3. (Secure if only \mathbf{R} cheats.) *Suppose \mathbf{P} and \mathbf{S} follow \mathcal{P} honestly, but \mathbf{R} potentially deviates. Let $\rho_{\text{cq}}^{\mathbf{R}}(\tilde{\mathbf{x}}, \tilde{\mathbf{y}})$ denote the total cq state held by \mathbf{R} at the end of \mathcal{P} , given inputs $(\tilde{\mathbf{x}}, \tilde{\mathbf{y}})$ of \mathbf{P} and \mathbf{S} , respectively. Then, there exists a simulator \mathbb{S} for \mathbf{R} interacting with the ideal functionality f_{ideal} that exactly reproduces $\rho_{\text{cq}}^{\mathbf{R}}(\tilde{\mathbf{x}}, \tilde{\mathbf{y}})$ for all $(\tilde{\mathbf{x}}, \tilde{\mathbf{y}})$.*

Scenario I: Honest \mathbf{P} and \mathbf{R} . The first scenario we consider involves \mathbf{P} and \mathbf{R} participating honestly in \mathcal{P} , while \mathbf{S} is a potentially malicious adversary. \mathcal{P} involves independent local measurements on each copy of $|G_i\rangle$ by the honest participants. Let $\tilde{\mathbf{x}}$ be any fixed input of the function f for \mathbf{P} . We consider two subcases where \mathbf{S} takes on the role of either \mathbf{A}_i or \mathbf{B}_i in any arbitrary iteration i in Stage I of \mathcal{P} .

- (a) **Honest \mathbf{R} and \mathbf{B}_i .** Following \mathcal{P} , the post-measurement state of $|G_i\rangle$ can be easily expressed in the stabilizer formalism. Once qubits (1, 6, 10) are measured by \mathbf{B}_i and (3, 7, 9) by \mathbf{R} , the post-measurement state following \mathbf{B}_i 's rotation $Z_8^{m_{i,6}}$ is described by a stabilizer with generators

$$\begin{aligned} S_{\mathbf{A}_i, 8, 12} = & \langle (-1)^{m_{i,1}+m_{i,3}} X_2, (-1)^{m_{i,6}+m_{i,7}} Z_5, \\ & (-1)^{m_{i,3}} X_4 Z_{12}, (-1)^{m_{i,6}+m_{i,7}} X_8 Z_{12}, (-1)^{m_{i,9}} X_{11} Z_{12}, Z_4 Z_8 Z_{11} X_{12} \rangle. \end{aligned} \quad (\text{B2})$$

Note that subscript on S implies none of \mathbf{A}_i qubits have been measured yet, along with qubits (8, 12) of the honest parties. Next, \mathbf{B}_i and \mathbf{R} measure qubits 8 and 12, respectively. Their choice of measurement basis depends their common measurement outcome $s_i \equiv m_{i,9} = m_{i,10}$. The result is that \mathbf{A}_i is left with a state described by the generators

$$S_{\mathbf{A}_i} = \langle (-1)^{m_{i,1}+m_{i,3}} X_2, (-1)^{m_{i,6}+m_{i,7}} Z_5, (-1)^{m_{i,3}+s_i} X_4 X_{11}, (-1)^{(m_{i,6}+m_{i,7})s_i+m_{i,8}+m_{i,12}} Z_4 Z_{11} \rangle. \quad (\text{B3})$$

Thus, the state of \mathbf{A}_i 's qubits are completely determined by the correlations

$$\hat{m}_{i,2} \equiv m_{i,1} + m_{i,3}, \quad (\text{B4a})$$

$$\hat{m}_{i,4} \equiv m_{i,3} + s_i, \quad (\text{B4b})$$

$$\hat{m}_{i,5} \equiv m_{i,6} + m_{i,7} \quad (\text{B4c})$$

$$\hat{m}_{i,11} \equiv (m_{i,6} + m_{i,7})s_i + m_{i,8} + m_{i,12}, \quad (\text{B4d})$$

where we have used the notation, \hat{m} , to indicate the measurement outcomes \mathbf{A}_i could learn upon the appropriate stabilizer measurements. In the first part of Stage II, an honest \mathbf{B}_i broadcasts the message $c_{i,B} = m_{i,1} + b_i + 1$. We can therefore express $\hat{m}_{i,11}$ in terms of \mathbf{B}_i 's input and measurement outcomes as

$$\hat{m}_{i,11} = \hat{m}_{i,5}(\hat{m}_{i,2} + \hat{m}_{i,4} + c_{i,B} + b_i + 1) + m_{i,8} + m_{i,12}, \quad (\text{B5})$$

where we have made the substitution $s_i = \hat{m}_{i,2} + \hat{m}_{i,4} + c_{i,B} + b_i + 1$. Finally, let $\hat{c}_{i,A} \in \{0, 1\}$ denote the message broadcast by a possibly malicious \mathbf{A}_i in this first part of Stage II, which can be computed in some non-specified way. For example, it could depend on some side information λ or any of the values in $\{\hat{m}_{i,2}, \hat{m}_{i,4}, \hat{m}_{i,5}, \hat{m}_{i,11}\}$. Honest \mathbf{B}_i then computes

$$\begin{aligned}\beta_i &= \hat{c}_{i,A} s_i + m_{i,8} \\ &= \hat{c}_{i,A} (\hat{m}_{i,2} + \hat{m}_{i,4} + c_{i,B} + b_i + 1) + m_{i,8}.\end{aligned}\quad (\text{B6})$$

The critical observation here is that due to the nature of measuring only Pauli observables on stabilizer states, the measurement outcomes $(m_{i,1}, m_{i,3}, m_{i,6}, m_{i,7}, s_i, m_{i,8}, m_{i,12})$ are independent and uniformly random bits. *Consequently, the bit values $(\hat{m}_{i,2}, \hat{m}_{i,4}, \hat{m}_{i,5}, \hat{m}_{i,11}, c_{i,B}, \beta_i)$ are also independent and uniformly random bits.* Hence, when \mathbf{S} plays the role of \mathbf{A}_i in \mathcal{P} , up to the first part of Stage II, the bit values they obtain are subsequently uncorrelated from \mathbf{B}_i 's input.

- (b) **Honest \mathbf{R} and \mathbf{A}_i .** Once qubits (2,5) are measured by \mathbf{A}_i and qubits (3,7,9) are measured by \mathbf{R} , the post-measurement state following \mathbf{A}_i 's rotation $Z_4^{m_{i,2}}$ is described by a stabilizer with generators

$$\begin{aligned}S_{\mathbf{B}_i,4,11,12} &= \langle (-1)^{m_{i,2}+m_{i,3}} Z_1, (-1)^{m_{i,5}+m_{i,7}} X_6, (-1)^{m_{i,9}} X_{10}, \\ &\quad (-1)^{m_{i,2}+m_{i,3}} X_4 Z_{12}, (-1)^{m_{i,7}} X_8 Z_{12}, (-1)^{m_{i,9}} X_{11} Z_{12}, Z_4 Z_8 Z_{11} X_{12} \rangle.\end{aligned}\quad (\text{B7})$$

Next, \mathbf{A}_i and \mathbf{R} measure qubits (4,11) and 12, respectively. \mathbf{A}_i 's measurement basis depends on her input a_i here, while the choice of \mathbf{R} 's depends on $s_i \equiv m_{i,9}$. The result is that \mathbf{B}_i is left with a state described by the generators

$$\begin{aligned}S_{\mathbf{B}_i} &= \langle (-1)^{m_{i,2}+m_{i,3}} Z_1, (-1)^{m_{i,5}+m_{i,7}} X_6, (-1)^{m_{i,9}} X_{10}, \\ &\quad (-1)^{a_i(m_{i,2}+m_{i,3}+s_i+1)+m_{i,7}s_i+m_{i,4}+m_{i,11}+m_{i,12}} W^{s_i} Z_8 (W^\dagger)^{s_i} \rangle.\end{aligned}\quad (\text{B8})$$

\mathbf{B}_i 's qubits are completely determined by the correlations

$$\hat{m}_{i,1} \equiv m_{i,2} + m_{i,3}, \quad (\text{B9a})$$

$$\hat{m}_{i,6} \equiv m_{i,5} + m_{i,7}, \quad (\text{B9b})$$

$$\hat{m}_{i,8} \equiv a_i(m_{i,2} + m_{i,3} + s_i + 1) + m_{i,7}s_i + m_{i,4} + m_{i,11} + m_{i,12}, \quad (\text{B9c})$$

$$\hat{m}_{i,10} \equiv s_i, \quad (\text{B9d})$$

where the measurement outcomes $(m_{i,2}, m_{i,3}, m_{i,4}, m_{i,5}, m_{i,7}, s_i, m_{i,11}, m_{i,12})$ are independent and uniformly random bits. In the first part of Stage II, honest \mathbf{A}_i broadcasts the message $c_{i,A} = m_{i,5} + a_i$. Let $\hat{c}_{i,B} \in \{0, 1\}$ denote the message \mathbf{B}_i broadcasts, which could depend on side information λ or any other information accessible to \mathbf{B}_i , and let $\alpha_i = a_i \hat{c}_{i,B} + m_{i,4} + m_{i,11}$. As before, *the bit values $(\hat{m}_{i,1}, \hat{m}_{i,6}, \hat{m}_{i,8}, \hat{m}_{i,10}, c_{i,A}, \alpha_i)$ are independent and uniformly random bits.* Hence, when \mathbf{S} plays the role of \mathbf{B}_i in \mathcal{P} , up to the first part of Stage II, the bit values they obtain are subsequently uncorrelated from \mathbf{A}_i 's input.

We now consider the second opening of Stage II, which combines all of the information \mathbf{S} has obtained from playing either \mathbf{A}_i or \mathbf{B}_i for various i . Let $\mathcal{A} \subset \{1, \dots, \mathfrak{R}\}$ denote the set of conjunctions in which \mathbf{P} assumed the role \mathbf{A}_i , and similarly, let $\mathcal{B} \subset \{1, \dots, \mathfrak{R}\}$ denote the set of conjunctions in which \mathbf{P} assumed the role of \mathbf{B}_i . Honest \mathbf{R} will broadcast the message $\Gamma_{\mathbf{R}} = \sum_{i=1}^{\mathfrak{R}} m_{i,12}$, while honest \mathbf{P} will broadcast

$$\begin{aligned}\Gamma_{\mathbf{P}} &\equiv z_{\mathbf{P}} + \sum_{i \in \mathcal{A}} \alpha_i + \sum_{i \in \mathcal{B}} \beta_i \\ &= z_{\mathbf{P}} + \sum_{i \in \mathcal{A}} (a_i \hat{c}_{i,B} + m_{i,4} + m_{i,11}) + \sum_{i \in \mathcal{B}} (\hat{c}_{i,A} (\hat{m}_{i,2} + \hat{m}_{i,4} + c_{i,B} + b_i + 1) + m_{i,8}).\end{aligned}\quad (\text{B10})$$

In total, all of the information (both classical and quantum) imparted to party \mathbf{S} at the end of \mathcal{P} is characterized by the bit values

$$\{\hat{m}_{i,1}, \hat{m}_{i,6}, \hat{m}_{i,8}, \hat{m}_{i,10}, c_{i,A} | i \in \mathcal{A}\} \cup \{\hat{m}_{i,2}, \hat{m}_{i,4}, \hat{m}_{i,5}, \hat{m}_{i,11}, c_{i,B} | i \in \mathcal{B}\} \cup \{\Gamma_{\mathbf{P}}, \Gamma_{\mathbf{R}}\} \quad (\text{B11})$$

As highlighted above, all the bits from the former two sets along with $\Gamma_{\mathbf{P}}$ are independent and uniformly random. However, $\Gamma_{\mathbf{R}}$ is completely determined by these bits and the inputs of \mathbf{P} due to the correlation

$$\begin{aligned}\Gamma_{\mathbf{P}} + \Gamma_{\mathbf{R}} + \sum_{i \in \mathcal{A}} \hat{m}_{i,11} + \sum_{i \in \mathcal{B}} \hat{m}_{i,8} &= z_{\mathbf{P}} + \sum_{i \in \mathcal{A}} (a_i (\hat{m}_{i,1} + \hat{c}_{i,B} + 1) + (\hat{m}_{i,6} + c_{i,A}) s_i) \\ &\quad + \sum_{i \in \mathcal{B}} (\hat{m}_{i,5} + \hat{c}_{i,A}) (\hat{m}_{i,2} + \hat{m}_{i,4} + c_{i,B} + b_i + 1).\end{aligned}\quad (\text{B12})$$

In other words, we have

$$\Gamma_{\mathbf{R}} = \sum_{i \in \mathcal{A}} \hat{m}_{i,11} + \sum_{i \in \mathcal{B}} \hat{m}_{i,8} = \left[z_{\mathbf{P}} + \sum_{i \in \mathcal{A}} a_i (\hat{m}_{i,1} + \hat{c}_{i,B} + 1) + \sum_{i \in \mathcal{B}} (\hat{m}_{i,5} + \hat{c}_{i,A}) b_i \right] + \zeta, \quad (\text{B13})$$

where

$$\zeta = \sum_{i \in \mathcal{A}} (\hat{m}_{i,6} + c_{i,A}) s_i + \sum_{i \in \mathcal{B}} (\hat{m}_{i,5} + \hat{c}_{i,A}) (\hat{m}_{i,2} + \hat{m}_{i,4} + c_{i,b} + 1). \quad (\text{B14})$$

Observe that the term in brackets is precisely $f(\tilde{\mathbf{x}}, \tilde{\mathbf{e}})$, where $\tilde{\mathbf{e}} = \{\hat{m}_{i,1} + \hat{c}_{i,B} + 1 | i \in \mathcal{A}\} \cup \{\hat{m}_{i,5} + \hat{c}_{i,A} | i \in \mathcal{B}\}$.

The simulation realized in Figure 6(a) is now straightforward. \mathbf{S} generates independently and uniformly random bits

$$\{\hat{m}_{i,1}, \hat{m}_{i,6}, \hat{m}_{i,8}, \hat{m}_{i,10}, c_{i,A} | i \in \mathcal{A}\} \cup \{\hat{m}_{i,2}, \hat{m}_{i,4}, \hat{m}_{i,5}, \hat{m}_{i,11}, c_{i,B} | i \in \mathcal{B}\} \cup \{\Gamma_{\mathbf{P}}\}. \quad (\text{B15})$$

For each such set of values, \mathbf{S} prepares a quantum states with stabilizers described by Equations (B3) and (B8). They then operate some quantum instrument \mathcal{I} and generate the variables $\{\hat{c}_{i,B} | i \in \mathcal{A}\}$ and $\{\hat{c}_{i,A} | i \in \mathcal{B}\}$ just as they would when cheating in \mathcal{P} , using their prepared quantum states and whatever other side information λ they have. What remains is a generation of $\Gamma_{\mathbf{R}}$ that has the same correlations with other variables as in \mathcal{P} . To accomplish this, \mathbf{S} first computes the value ζ in Equation (B14) using his sampled variables. He then computes $\tilde{\mathbf{e}}$ and uses this as his input to f , thereby obtains $f(\tilde{\mathbf{x}}, \tilde{\mathbf{e}})$. From Equation (B13), the correct value of $\Gamma_{\mathbf{R}}$ is given by the sum $f(\tilde{\mathbf{x}}, \tilde{\mathbf{e}}) + \zeta$.

Scenario II: Honest \mathbf{P} and \mathbf{S} . We now consider the post-measurement state left to \mathbf{R} , when \mathbf{P} and \mathbf{S} follow \mathcal{P} honestly. Once qubits (2, 8) and (1, 6, 9) are measured on a given copy of $|G_i\rangle$ and the appropriate rotations are performed by \mathbf{A}_i and \mathbf{B}_i , respectively, this post-measurement state is described by generators

$$S_{\mathbf{R},4,8,11} = \langle (-1)^{m_{i,2}} X_3, (-1)^{m_{i,6}} X_7, (-1)^{s_i} X_9, \\ (-1)^{m_{i,1}} X_4 Z_{12}, (-1)^{m_{i,5}} X_8 Z_{12}, (-1)^{s_i} X_{11} Z_{12}, Z_4 Z_8 Z_{11} X_{12} \rangle, \quad (\text{B16})$$

where $s_i \equiv m_{i,10}$. Next, \mathbf{A}_i and \mathbf{B}_i measure qubits (4, 11) and 8, respectively, following the prescription of \mathcal{P} . The state of \mathbf{R} is then described by generators

$$S_{\mathbf{R}} = \langle (-1)^{m_{i,2}} X_3, (-1)^{m_{i,6}} X_7, (-1)^{s_i} X_9, (-1)^{a_i(m_{i,1}+s_i+1)+m_{i,5}s_i+m_{i,4}+m_{i,8}+m_{i,11}} V^{s_i} X_{12} (V^\dagger)^{s_i} \rangle. \quad (\text{B17})$$

As before, \mathbf{R} 's qubits are completely determined by the correlations

$$\hat{m}_{i,3} \equiv m_{i,2}, \quad (\text{B18a})$$

$$\hat{m}_{i,7} \equiv m_{i,6}, \quad (\text{B18b})$$

$$\hat{m}_{i,9} \equiv s_i, \quad (\text{B18c})$$

$$\hat{m}_{i,12} \equiv a_i(m_{i,1} + s_i + 1) + m_{i,5}s_i + m_{i,4} + m_{i,8} + m_{i,11}. \quad (\text{B18d})$$

In the first part of Stage II, \mathbf{R} learns the values $c_{i,A}$ and $c_{i,B}$, as they are defined in \mathcal{P} . In the second part, \mathbf{R} learns

$$\Gamma_{\mathbf{P}} = z_{\mathbf{P}} + \sum_{i \in \mathcal{A}} (a_i c_{i,B} + m_{i,4} + m_{i,11}) + \sum_{i \in \mathcal{B}} c_{i,A} s_i + m_{i,8}, \quad (\text{B19a})$$

$$\Gamma_{\mathbf{S}} = z_{\mathbf{S}} + \sum_{i \in \mathcal{A}} c_{i,A} s_i + m_{i,8} + \sum_{i \in \mathcal{B}} (a_i c_{i,B} + m_{i,4} + m_{i,11}). \quad (\text{B19b})$$

The variables $\{\hat{m}_{i,3}, \hat{m}_{i,7}, \hat{m}_{i,9}, \hat{m}_{i,12} | i = 1, \dots, \mathfrak{R}\}$ are jointly independent with $\Gamma_{\mathbf{P}}$. However, $\Gamma_{\mathbf{S}}$ is completely determine by them and the inputs of \mathbf{P} and \mathbf{S} , as there exists the correlation

$$\Gamma_{\mathbf{P}} + \Gamma_{\mathbf{S}} + \sum_{i=1}^{\mathfrak{R}} \hat{m}_{i,12} = z_{\mathbf{P}} + z_{\mathbf{S}} + \sum_{i=1}^{\mathfrak{R}} a_i b_i = f(\tilde{\mathbf{x}}, \tilde{\mathbf{y}}). \quad (\text{B20})$$

Hence, the simulation realizing Figure 6(b) is also straightforward. \mathbf{R} first generates independent and uniformly random bits $\{\hat{m}_{i,3}, \hat{m}_{i,7}, \hat{m}_{i,9}, \hat{m}_{i,12} | i = 1, \dots, \mathfrak{R}\} \cup \{\Gamma_{\mathbf{P}}\}$ and prepares the state with the generators in Equation (B17). Then for any pair of inputs $(\tilde{\mathbf{x}}, \tilde{\mathbf{y}})$ from \mathbf{P} and \mathbf{S} and public evaluation of the function $f(\tilde{\mathbf{x}}, \tilde{\mathbf{y}})$, \mathbf{R} computes $\Gamma_{\mathbf{S}}$ from Equation (B20).

2. Including error correction

In practice, each bit conjunction computed in Stage I of the will have some error. In this section we describe a basic error correction method that can be employed to suppress the overall computational error as much as desired.

Let ϵ_* denote the largest probability of a bit error in each iteration of Stage I, and let Ξ_i be the indicator variable for the occurrence of an error in iteration i . Thus, while the noiseless protocol generates bit values $a_i b_i = m_{i,12} + \alpha_i + \beta_i$ in iteration i , the actual implementation generates bit values

$$a_i b_i = m_{i,12} + \alpha_i + \beta_i + \Xi_i. \quad (\text{B21})$$

To deal with this, the Referee can employ a simple repetition code. That is, each iteration i is repeated K times, from which the Referee obtains values $m_{(i,1),12}, m_{(i,2),12}, \dots, m_{(i,K),12}$, where

$$m_{(i,j),12} = a_i b_i + \alpha_{(i,j)} + \beta_{(i,j)} + \Xi_{(i,j)}. \quad (\text{B22})$$

Recalling that $\alpha_{(i,j)}$ and $\beta_{(i,j)}$ are Alice and Bob's private bits, for each $j = 2, \dots, K$, Alice and Bob open the messages $\alpha_{(i,1)} + \alpha_{(i,j)}$ and $\beta_{(i,1)} + \beta_{(i,j)}$, respectively. The Referee adds these to each corresponding $m_{(i,j),12}$ so that his K bit values then have the form

$$m_{(i,j),12} = a_i b_i + \alpha_{(i,1)} + \beta_{(i,1)} + \Xi_{(i,j)}. \quad (\text{B23})$$

Note that each $\alpha_{(i,j)}$ and $\beta_{(i,j)}$ is an independent private random bit for Alice and Bob, so the announcements of $\alpha_{(i,1)} + \alpha_{(i,j)}$ and $\beta_{(i,1)} + \beta_{(i,j)}$ do not reveal any information about $\alpha_{(i,1)}$ and $\beta_{(i,1)}$.

The Referee then performs majority voting on the bit values $m_{(i,j),12}$, accepting the value appearing the most among the K sub-iterations. By Hoeffding's inequality, this value will be $m_{i,12} = a_i b_i + \alpha_i + \beta_i$ with a bit error rate $\delta \leq \exp[-2K(\frac{1}{2} - \epsilon_* - \frac{1}{2K})^2]$. Then, the combined bit error rate in computing $\Gamma_{\mathbf{R}} = \sum_{i=1}^{\mathfrak{R}} m_{i,12}$ is equal to the probability that an odd number of bit errors occur among the $m_{(i,j),12}$. A counting argument shows this probability to be

$$\epsilon = \frac{1}{2}[1 - (1 - 2\delta)^{\mathfrak{R}}] \leq \delta \mathfrak{R} \leq \mathfrak{R} \cdot \exp[-2K(\frac{1}{2} - \epsilon_* - \frac{1}{2K})^2]. \quad (\text{B24})$$

Note that to suppress the bit error rate, the number of repetitions K needed for each iteration i is exponentially smaller than the total number of iterations $\mathfrak{R} \leq \binom{N}{2}(M-1)^2$. In particular, to obtain a bit error probability ϵ_f on the computation of f for fixed ϵ_* , it suffices to take

$$K = \left\lceil \frac{1}{(\frac{1}{2} - \epsilon_*)^2} \ln \sqrt{\frac{\mathfrak{R}_1}{\epsilon_f}} \right\rceil \leq \left\lceil \frac{1}{(\frac{1}{2} - \epsilon_*)^2} \ln \left(\frac{(M-1)N}{\sqrt{2\epsilon_f}} \right) \right\rceil. \quad (\text{B25})$$

In total, the N -party computation of f on each party's M -bit input can be implemented with error correction in our protocol at a lower bound unit rate of

$$\frac{R}{R_0} \geq \left(4(M-1)N \left[\frac{\ln((M-1)N/\sqrt{2\epsilon_f})}{(\frac{1}{2} - \epsilon_*)^2} \right] \right)^{-1}, \quad (\text{B26})$$

where R_0 is the scheme-dependent average rate to add a new photon to a graph state. For the HoD scheme we propose, $R_0 = \eta_e R_{\text{rep}}$.

3. Self-testing of graph states

We can further secure the computation against an untrustworthy Source, via a self-testing procedure, which allows the parties and the Referee to validate the state distributed by the Source. If the parties indeed have the correct state, measuring the independent components of a uniformly randomly chosen stabilizer of the state will lead to a correlated outcome, hence implementing a partial test of the state's validity. By repeating the protocol and partitioning rounds between these stabilizer tests, discarded rounds of computation, and a single accepted target round of computation, the parties can upper bound the probability of receiving the incorrect state during the target round [58]. In implementing our multi-party protocol within our HoD scheme for generating the requisite states, we require the set of instructions, detailing which rounds to test, compute, and ultimately accept, be a private source of shared randomness between the

parties and the Referee. This could be generated initially from a set of GHZ states distributed to the participants in the computation [65]. Without knowledge of which rounds are stabilizer tests and which are computations, the Source is prevented from modifying the state they distribute in order to fool the participants during rounds of self-testing. Conversely, the HoS scheme allows for the requisite graph states to be produced prior to the measurement-based computation protocol. Hence, the instruction set directing the participants when to self-test can be decided after the state has already been generated. In these schemes, we therefore do not require a distinct Source and Referee, at the cost of necessitating memory—in requiring the full set of photonic states be generated in advance, as well as additional rounds of self-testing [59].

Appendix C: Constructing graph states with “emit then add”

Building graph states in either of the HoS and HoD schemes necessitates additional experimental overhead from typical deterministic quantum emitter-based schemes, in both the number of qubits required and entangling operations between them. We demonstrate through an inductive argument that these additional resource costs scale at worst linearly. Subsequently, we present a resource-efficient set of subroutines used to produce the requisite states for our multi-party computation protocol, described in Section V. As the whole of our protocol is Clifford, we can employ the HoD scheme to produce and measure these graph states efficiently in practice, without the need for a quantum memory. We briefly discuss how phase corrections, resulting from these construction subroutines, are handled classically in this scheme. The subroutines we introduce are thereafter employed in Appendix D to estimate the fidelity to make the states used in our protocol. In what follows, a superscript (p) , (s) , or (e) denotes the kind of physical qubit associated with the relevant subspace on which an operator acts, as a photon, auxiliary spin, or emitter, respectively.

1. Additional overhead

Let $|G\rangle$ define an existing graph state in which there is at least a single edge between an auxiliary spin and the set of photons previously added to the graph. We label each of these photons by an emission order $1, \dots, m-1$. Let V_m define the additional vector space describing the emitter and the next photon, m , to be added to the graph, both of which start in $|0\rangle$. The set of generators which stabilizes the collective vector space $V_G + V_m$, consisting of the graph and subsequent emitter-photon pair, has the form

$$S_{V_G+V_m} = \langle \dots, \dots Z_k^{(p)} \dots X^{(s)}, Z^{(e)}, Z_m^{(p)} \rangle, \quad (\text{C1})$$

where $\langle \dots \rangle$ denotes a set of generators and the notation $\dots Z_k^{(p)} \dots$ is used to keep track of an arbitrary edge between the auxiliary spin and a photon previously added to the graph at some emission step $k < m$. The subcircuit depicted in Figure 9 demonstrates an example of how to transfer entanglement (or conditional phase information) from the emitter-photon sub-system to $|G\rangle$, with a single two-qubit spin-spin entangling gate and local complementation. In implementing the example, we transform the stabilizer of the combined vector space in Equation (C1) as

$$S'_{V_G+V_m} = \langle \dots, (-1)^{c_m} \dots Z_k^{(p)} \dots X_m^{(p)} X^{(s)}, (-1)^{c_m} Z_m^{(p)} Z^{(s)}, (-1)^{c_m} Z^{(e)} \rangle \quad (\text{C2})$$

where $c_m \in \{0, 1\}$ is a classical bit value conditioned on the measurement of the emitter.

The result of these operations produces the same stabilizer we would have arrived at had we instead pumped the auxiliary spin itself. With these additional operations, any graph state accessible in the deterministic scheme can be constructed in the HoS or HoD schemes. As we restrict those auxiliary spins already entangled with any previously added photons from being pumped, it follows that one additional spin, the emitter, and one two-qubit spin-spin entangling gate per photon in G are the minimum additional overhead in our proposed schemes for making arbitrary graph states. Furthermore, we can define a new vector space V'_G , containing the existing graph state and a newly entangled photon, with a dimension that increases by one with each new photon. The new space V'_G is stabilized by a unique set of generators that can be rotated back to a graph state basis of the same general form as Equation (C1), now defined by a new graph state $|G'\rangle$.

2. Construction subroutines

We also offer a pair of subroutines that simplifies the construction and overhead for the graph states $|G_I\rangle$ and $|G_{II}\rangle$, described in Section V. Representations of the graph transformations associated with the two subroutines, along with

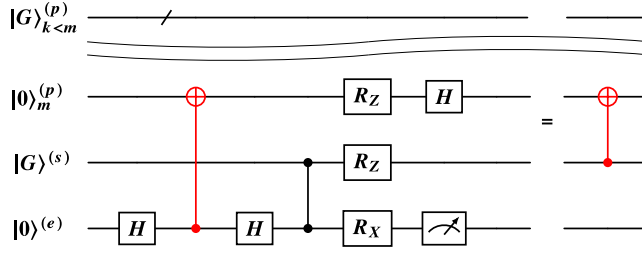


FIG. 9. A subcircuit equivalent to a $CX_{s,p}$ gate, up to a conditional phase correction, for transferring entanglement (conditional phase information) in our proposed HoS (HoD) scheme. This example “emit then add” procedure replaces every pumping gate in typical deterministic schemes for generating arbitrary photonic graph states. Entanglement (conditional phase information) between a photon (p) and a coherently pumped emitter (e) (represented by a red $CX_{e,p}$ gate) is exchanged to an auxiliary spin (s) via a two-qubit entangling $CZ_{e,s}$ gate and local complementation. The emitter is measured out thereafter and reinitialized for the next iteration of the procedure. Rotations about X and Z are by $\pi/2$ and $-\pi/2$, respectively, as noted in Equation (A7). The measurement of the emitter is with respect to the Z basis. All previously added photons at iterations $k < m$ are unaffected.

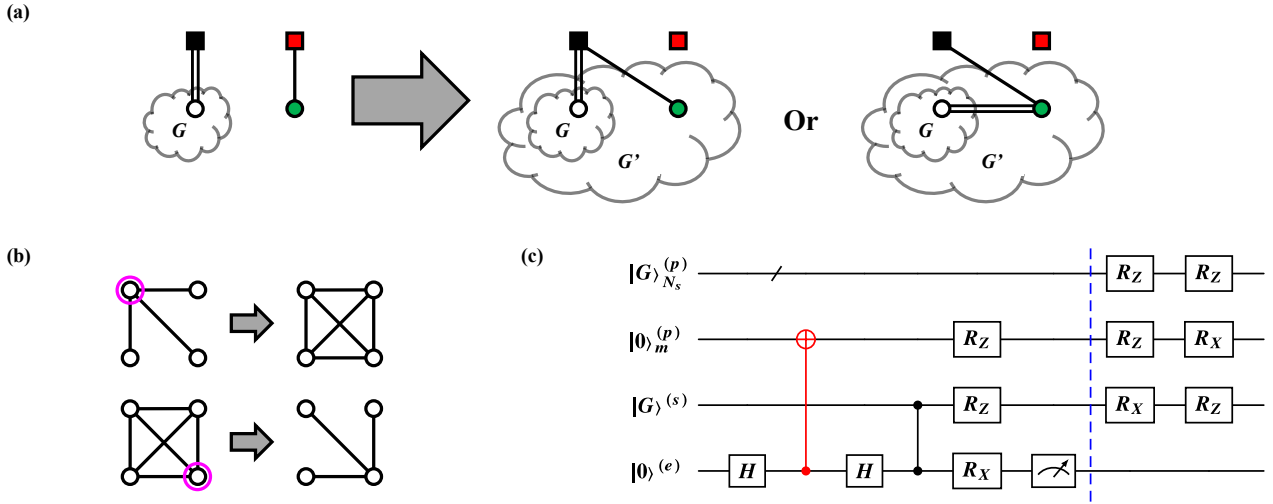


FIG. 10. Passing-subroutine for adding new photons to an existing graph, G . (a) A graph transformation of passing a new photon (green) from the emitter (red) to an auxiliary spin (black), which is connected to one or more previously added photons (white, denoted with a double edge for the multiplicity). This subroutine consists of two variations: (left) leaving all previously added photons invariant, (right) transplanting those edges to the newly added photon. (b) An example of how local complementations on a target qubit (magenta circle) can be used to add or remove edges. (c) A quantum subcircuit which implements the graph transformation. The right variation of the graph transformation above is achieved with the additional two local complementations (blue dashed line, depicting the deviation). Rotations and measurements follow the same notation as in Figure 9.

example circuits, are depicted in Figures 10 and 11. These transformations can be performed successively with no additional operations, transforming the previous graph G built on the auxiliary spin to a new graph G' with any new photons sharing an edge to the auxiliary spin. Despite their intended application in our MPC protocol, we make no assumptions about the measurement of the photons in these subroutines, such that they can be applied generally across experimental implementations.

One “passing”-subroutine, shown in Figure 10 consists of two variations: “join” and “extend”. The join-subroutine adds a new photon to an existing graph and leaves all previously existing edges invariant. The extend-subroutine transfers all edges from the auxiliary spin to the new photon. The two are achieved without or with the additional two local complementations depicted at the end of the example circuit, respectively. Both variations only act on previously added photons in the neighborhood of the auxiliary spin, N_s . Repeatedly applying the join-subroutine or extend-subroutine on a single auxiliary spin produces a star graph or linear cluster state, respectively for each

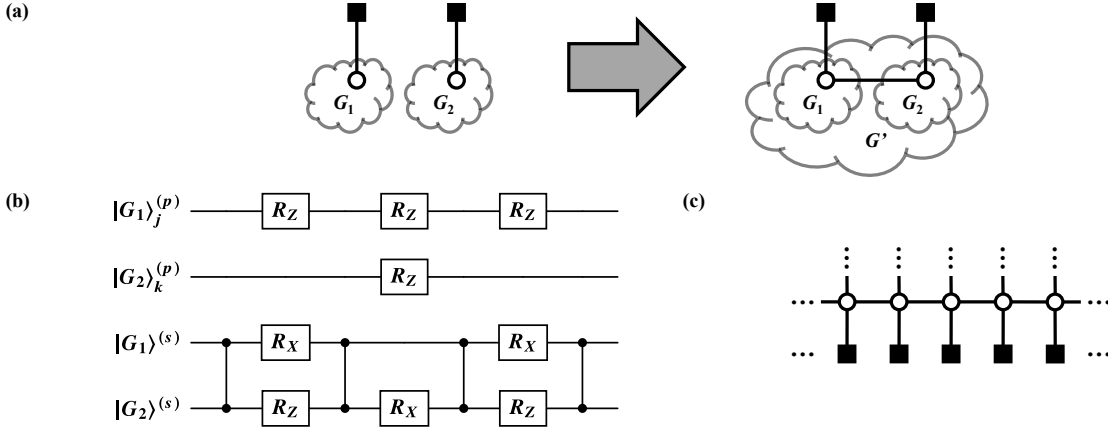


FIG. 11. Patching-subroutine for attaching two subgraphs G_1 and G_2 by a common edge between photons. (a) The graph transformation depicting the patching. (b) The corresponding circuit diagram. Additional two-qubit spin-spin entangling gates are required for this subroutine, over the passing-subroutine. Rotations follow the same notation as in Figure 9. (c) A 2D cluster state built on an array of auxiliary spins. Edges can be generated between photons in the layer neighboring the array of spins with this patching.

variation. Additionally, either variation of this subroutine can be appropriately implemented between auxiliary spins to connect subgraphs.

We note briefly that in practice with each implementation of the passing-subroutine, the newly added photon to the graph carries a conditional phase that is a byproduct of the decoupling measurement made on the emitter, as shown in Equation (C2). This byproduct phase determines the precise basis state of the graph and may require correction for general MBQCs. In the HoD scheme, photons are measured before they are decoupled from the emitter and hence any requisite phase corrections need be commuted after each measurement. The Clifford nature of the computations employed in our MPC simplifies all of these corrections to bit flips that can be handled classically. Furthermore, correction of this phase is not always necessary as certain measurements made by the parties destroy this phase information, while other measurements allow the parties to absorb this phase information into their own pad. Conversely, conditional measurements, such as the ones made by Alice in step (4) of Stage I of \mathcal{P} , couple these byproduct phases to the phase information input into the computation. Therefore, classical communication is required here between Alice and the Source. A simple solution is for the Source to make public the outcomes of each of these decoupling measurements.

The other “patching”-subroutine, shown in Figure 11, serves to attach two subgraphs G_1 and G_2 by a common edge between photons. This process requires additional two-qubit spin-spin entangling gates from the passing-subroutine. For further simplicity we only consider the case where G_1 and G_2 each have a single edge to all previously added photons in their respective subgraphs, though in general this subroutine fully connects all of the photons at the first layer in each subgraph. Operations in this subroutine are restricted locally to only the emitter, spin, and the photons we ultimately require to share an edge, labeled in the figure by arbitrary emission steps j, k in $1, \dots, n_p$. This subroutine mirrors the one employed in the production of large 2D cluster states in [5], and can be applied in either scheme we propose for the same purpose.

Application of these subroutines to the construction of the graph state discussed in Section V is straightforward. The state $|G\rangle$, consisting of $n_p = 12$ photons, labeled by an emission ordering depicted in Figure 5, can be built following the sequence of steps in the Build below. This procedure requires 17 two-qubit spin-spin entangling gates in total: 13 from passing operations, and 4 from a single patching steps. It is known that the sequential nature of photon emission events imparts an ordering on the graph state, limiting the kinds of photonic graphs accessible by construction on a single quantum emitter [66]. The private nature of the padded bit conjunctions in Stage I sets a nontrivial emission ordering on $|G\rangle$, which, following the results of [37], requires two auxiliary spins to construct.

Build $|G\rangle$:

Input: A photon emission order labeling photons $(p_1), \dots, (p_{12})$, corresponding to the $n_p = 12$ photons in $|G\rangle$, an emitting spin, and two auxiliary spins, labeled (s_1) and (s_2) .

1. Pass photons (p_1) through (p_4) to (s_1) . Apply the join-subroutine for (p_4) and the extend-subroutine for the

rest.

2. Pass photons (p_5) through (p_8) to (s_2) . Apply the join-subroutine for (p_5) and the extend-subroutine for the rest.
3. Pass the subgraph on (s_2) to (s_1) with the join-subroutine.
4. Pass photons (p_9) through (p_{12}) to (s_2) . Apply the join-subroutine for (p_9) and the extend-subroutine for the rest.
5. Patch the subgraph on (s_2) with (s_1) . Measure out both (s_1) and (s_2) .

Appendix D: Experimentally realizable fidelity calculations

We now consider an experimental realization of our schemes for constructing the graph states utilized in our multi-party computation. While the nature of the herald and the computation itself are device-independent, we assume here trapped ions as our quantum emitters and auxiliary spins, due to their high-fidelity benchmarks for two-qubit spin-spin entangling gates [14, 15] and reasonable collection efficiency with high-NA optics [16]. We outline our fidelity model for two schemes; the HoS scheme involving the heralding of a Bell state between an emitter and a photon for general cases involving non-destructive heralding of photons, and the HoD scheme where emitter photons are measured directly in the basis required for the measurement-based computation protocol.

1. Experimental apparatus

For the HoS scheme, heralding a Bell state between an emitter and photon is implemented via entanglement swapping between a photon from an emitter and a photon from a nonlinear pair source. We use spontaneous parametric down conversion (SPDC) as our pair source for the heralding. SPDC is an optical process based on a crystal with $\chi^{(2)}$ nonlinearity whereby a photon from a pump is converted to a signal and idler photon pair of lower energy. It is often used to produce entangled photon pairs in various degrees of freedom, or as a heralded single photon source [33]. The joint measurement apparatus required for the entanglement swapping in the heralding scheme we describe here can be accomplished via a generalized Hong-Ou-Mandel interferometer [67] depicted in Figure 12(a), where the emitter photon and signal photon from the pair source are sent to a 50:50 beamsplitter. Elements from these experiments are modeled in our estimates of the fidelity to successfully produce graph states.

We briefly consider the set of states employed in heralding a Bell state in a device-independent form. The internal state of an emitter (e) is entangled with a photon (p_e) in an arbitrary basis, and an entangled photon pair is produced from the SPDC source labeled as the signal (p_s) and idler (p_i) photons. We can express both the idealized entangled states $|\Psi_E\rangle$ and $|\Psi_P\rangle$, respectively, as

$$|\Psi_E\rangle = \frac{1}{\sqrt{2}}(|0\rangle^{(e)} |1; 0\rangle^{(p_e)} - |1\rangle^{(e)} |0; 1\rangle^{(p_e)}), \quad (\text{D1})$$

$$|\Psi_P\rangle = \frac{1}{\sqrt{2}}(|1; 0\rangle^{(p_s)} |0; 1\rangle^{(p_i)} - |0; 1\rangle^{(p_s)} |1; 0\rangle^{(p_i)}), \quad (\text{D2})$$

where $|0\rangle^{(e)}$ and $|1\rangle^{(e)}$ is the computational basis for the emitter, and the notation $|m; n\rangle$ is used to denote the photonic Fock state representation for a particular basis $\{|u\rangle, |v\rangle\}$, such as orthogonal polarizations, with m in $|u\rangle$ and n in $|v\rangle$. The relationship between the input modes a and b and output modes c and d of the 50:50 beamsplitter can be described by the unitary transformation on the creation operators $\hat{a}^\dagger = \frac{1}{\sqrt{2}}(\hat{c}^\dagger + \hat{d}^\dagger)$ and $\hat{b}^\dagger = \frac{1}{\sqrt{2}}(\hat{c}^\dagger - \hat{d}^\dagger)$. With the emitter photon entering port a , and the signal photon entering port b , the overall state after applying the transformation can be expressed in the form

$$\begin{aligned} |\Psi_E\rangle |\Psi_P\rangle &= \frac{(\hat{c}_u^\dagger)^2 - (\hat{d}_u^\dagger)^2}{4} |vac\rangle_{c,d} |0\rangle^{(e)} |0; 1\rangle^{(p_i)} + \frac{\hat{d}_u^\dagger \hat{d}_v^\dagger - \hat{c}_u^\dagger \hat{c}_v^\dagger}{2\sqrt{2}} |vac\rangle_{c,d} |\Psi^+\rangle^{(e,p_i)} \\ &+ \frac{\hat{c}_u^\dagger \hat{d}_v^\dagger - \hat{c}_v^\dagger \hat{d}_u^\dagger}{2\sqrt{2}} |vac\rangle_{c,d} |\Psi^-\rangle^{(e,p_i)} + \frac{(\hat{c}_v^\dagger)^2 - (\hat{d}_v^\dagger)^2}{4} |vac\rangle_{c,d} |1\rangle^{(e)} |1; 0\rangle^{(p_i)}, \end{aligned} \quad (\text{D3})$$

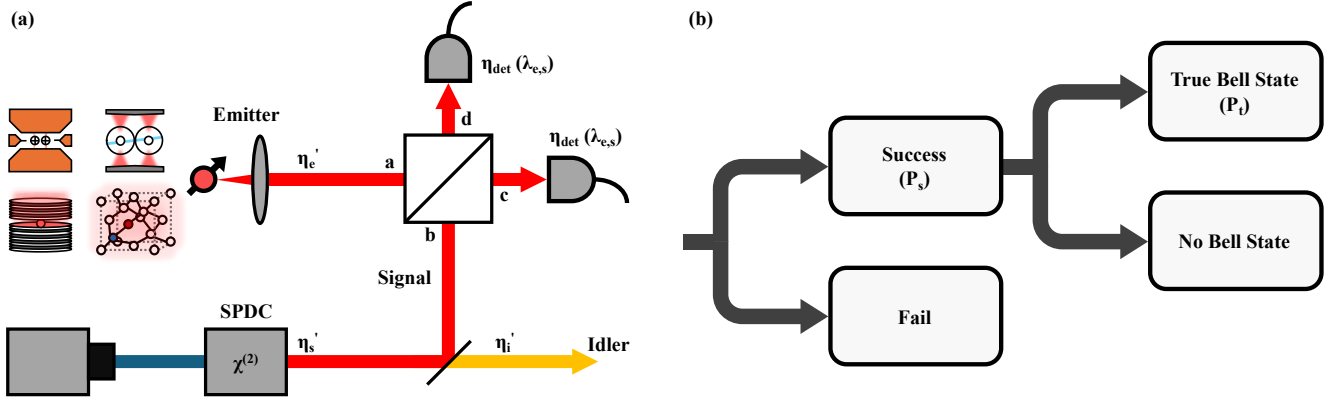


FIG. 12. Entanglement swapping in the HoS scheme. (a) Schematic of a generalized Hong-Ou-Mandel interferometer applied as a joint measurement apparatus. A photon entangled with an emitter is sent through port a of the beamsplitter, and a photon from a spontaneous parametric down conversion (SPDC) photon pair source is sent through port b . Detection of two single-photon orthonormal states $|u\rangle, |v\rangle$ in either output ports c or d results in entanglement between the emitter and the idler photon from the pair source. Various loss factors denoted by η are modeled. Additional elements for qubit rotations are not shown. (b) Probability tree showing the outcomes of a Bell state measurement attempt. The “success” probability P_s for the Bell state measurement denotes the probability of measuring a set of specific click patterns that indicate entanglement swapping. P_t denotes the probability of projecting the emitter and idler onto a Bell state per measurement attempt.

where

$$|\Psi^\pm\rangle^{(e,p_i)} = \frac{1}{\sqrt{2}}(|0\rangle^{(e)}|1;0\rangle^{(p_i)} \pm |1\rangle^{(e)}|0;1\rangle^{(p_i)}). \quad (\text{D4})$$

We are interested in projecting onto either $|\Psi^+\rangle^{(e,p_i)}$ or $|\Psi^-\rangle^{(e,p_i)}$ which can be realized by detecting specific click patterns on photon counting detectors at the output ports capable of resolving the orthonormal components. From Equation (D3), we can see that detecting orthonormal one-photon states in either ports c or d results in a projection onto $|\Psi^+\rangle^{(e,p_i)}$ while detection in opposite ports results in $|\Psi^-\rangle^{(e,p_i)}$. The overall probability of projection onto either of the Bell states is $\frac{1}{2}$ for each heralded measurement attempt. Upon the detection of $|\Psi^-\rangle^{(e,p_i)}$, we can perform a qubit rotation to produce the state $|\Psi^+\rangle^{(e,p_i)}$ for phase consistency. We can then perform a series of one- and two-qubit gates to add a photon to a graph. Upon failure to detect the correct detection pattern, we reinitialize the emitter and photon pair and attempt the measurement again. We assume number-resolving detectors at the output ports of the beamsplitter capable of detecting photons in the basis $\{|u\rangle, |v\rangle\}$. For example, two polarizing beamsplitters and four detectors would be used after the output ports for photons entangled in a polarization basis.

The initial state of the emitter can be described by the state defined in Equation (D1). The output state of SPDC is a multi-mode squeezed state where the photon pair production probability is dependent on the pump amplitude. Assuming a classical pump, we take the Hamiltonian for the SPDC process to approximately be of the form [38, 68]

$$\hat{H} = e^{i\phi}\kappa\hat{K}^\dagger + e^{-i\phi}\kappa\hat{K}, \quad (\text{D5})$$

where $\hat{K}^\dagger = \hat{a}_{u;s}^\dagger\hat{a}_{v;i}^\dagger - \hat{a}_{v;s}^\dagger\hat{a}_{u;i}^\dagger$ represents the creation of entangled signal and idler pairs denoted s and i in the basis $\{|u\rangle, |v\rangle\}$. The time evolution operator $\hat{U}(t) = \exp(i\hat{H}t/\hbar)$ yields the resulting state

$$|\Psi_{SPDC}\rangle = N \sum_{n=0}^{\infty} \tanh^n r \sum_{m=0}^n (-1)^m |n-m; m\rangle^{(p_s)} |m; n-m\rangle^{(p_i)}, \quad (\text{D6})$$

where $r = \kappa t/\hbar$ is the interaction parameter that is dependent on the pump field amplitude, t is the interaction time of the pump through the crystal, and N is the normalization constant with $N = 1 - \tanh^2 r$. By tuning the interaction parameter r , we can change the probability of producing a single pair ($n = 1$ in Equation (D6) leading to Equation (D2)) to optimize the fidelity of the HoS scheme. Note that increasing the pump power also increases the relative contribution of the higher order terms ($n > 1$), which increases the probability of detecting multiple photon pairs.

The above is applicable for polarization-entangled photon pairs directly produced in type-II SPDC described in refs. [38, 68]; the output state and choice of degree-of-freedom for entanglement will of course be dependent on the specific properties of the photon pair source and pump. However, we note that we are assuming the pump can be treated as a classical, single-mode source, and we use a simplified Hamiltonian and output state for the photon pairs entangled in $\{|u\rangle, |v\rangle\}$. Moreover, factors such as the multi-modal nature of the pump, phase differences or instabilities between the orthonormal components in the optical path, or distinguishability between the photons from the emitter and the SPDC source can degrade the fidelity of the scheme.

2. Sources of infidelity

Several experimentally relevant sources of infidelity are considered in our model. Photonic loss and detector dark counts can induce false heralding events, leading to a failure to resolve a true Bell state and subsequent addition of a photon to the graph. Decoherence across the emitter and any auxiliary spins utilized in building the graph will produce errors on any computation done on the graph state. The fidelity of each two-qubit spin-spin entangling gate performed in the construction is considered as well. We can also consider the fidelity of the initial entanglement between the emitter and its photon, as well as the entanglement of the photon pair, used in the entanglement swapping procedure.

a. Photonic loss

We use the standard approach to modeling photonic losses, which is to introduce a fictitious beamsplitter with transmittance η and reflectance $1 - \eta$ on the lossy channel. This is equivalent to applying the transformation on the creation operator $\hat{a}^\dagger = \sqrt{\eta}\hat{a}_T^\dagger + \sqrt{1 - \eta}\hat{a}_R^\dagger$ [69] where T and R denote the transmitted and reflected paths, respectively. The Fock state $|n\rangle$ serving as the input transforms as $|n\rangle \rightarrow \sum_{k=0}^n \sqrt{\binom{n}{k}\eta^{n-k}(1-\eta)^k} |n-k\rangle_T |k\rangle_R$ and the reflected path is traced out. We assume, for simplicity, that η is independent of the photonic degrees of freedom for each loss channel modeled. Applying this to an emitter with an initial state given by Equation (D1) and performing the partial trace over the reflected path, the resulting density matrix $\hat{\rho}_E$ for the emitter-photon pair incorporating losses is

$$\begin{aligned} \hat{\rho}_E = & \frac{1}{2}(1 - \eta_e) |0\rangle\langle 0|^{(e)} \otimes |vac\rangle\langle vac|^{(p_e)} + \frac{1}{2}(1 - \eta_e) |1\rangle\langle 1|^{(e)} \otimes |vac\rangle\langle vac|^{(p_e)} \\ & + \frac{1}{2}\eta_e |0\rangle\langle 0|^{(e)} \otimes |1; 0\rangle\langle 1; 0|^{(p_e)} + \frac{1}{2}\eta_e |1\rangle\langle 1|^{(e)} \otimes |0; 1\rangle\langle 0; 1|^{(p_e)} \\ & - \frac{1}{2}\eta_e |0\rangle\langle 1|^{(e)} \otimes |1; 0\rangle\langle 0; 1|^{(p_e)} - \frac{1}{2}\eta_e |1\rangle\langle 0|^{(e)} \otimes |0; 1\rangle\langle 1; 0|^{(p_e)}. \end{aligned} \quad (D7)$$

Similarly, the density matrix for the SPDC source $\hat{\rho}_{SPDC}$ becomes

$$\begin{aligned} \hat{\rho}_{SPDC} = & \sum_{n, n^*=0}^{\infty} \sum_{m=0}^n \sum_{m^*=0}^{n^*} \sum_{k_s, k'_s=0}^{\min\{n-m, n^*-m^*\}} \sum_{k_i, k'_i=0}^{\min\{m, m^*\}} c_{n, m, k_s, k'_s, k_i, k'_i} c_{n^*, m^*, k_s, k'_s, k_i, k'_i}^* \\ & |n - m - k_s; m - k'_s\rangle \langle n^* - m^* - k_s; m^* - k'_s|^{(p_s)} \\ & \otimes |m - k_i; n - m - k'_i\rangle \langle m^* - k_i; n^* - m^* - k'_i|^{(p_i)}, \end{aligned} \quad (D8)$$

where

$$c_{n, m, k_s, k'_s, k_i, k'_i} = (1 - \xi)(\sqrt{\xi})^n (-1)^m \sqrt{\binom{n-m}{k_s} \binom{m}{k'_s} \binom{m}{k_i} \binom{n-m}{k'_i}} \eta_s^{n-k_s-k'_s} (1 - \eta_s)^{k_s+k'_s} \eta_i^{n-k_i-k'_i} (1 - \eta_i)^{k_i+k'_i}, \quad (D9)$$

and we have used $\xi = \tanh^2 r$. Here, we have made the additional substitutions $\eta_e = \eta'_e \eta_{det}(\lambda_e)$ and $\eta_s = \eta'_s \eta_{det}(\lambda_s)$, where η_e and η_s are the combined collection and photodetection efficiencies for the emitter and signal photons, respectively, in the interferometry setup. η' accounts for the collection efficiency of the optical path as shown in Figure 12(a), and $\eta_{det}(\lambda)$ is the photodetection efficiency which may be wavelength dependent (in the joint measurement, we require $\lambda_e = \lambda_s$). $\eta_i = \eta'_i$ is the collection efficiency of the idler for the SPDC setup, neglecting user-specific losses such as

transmission losses through an optical fiber network and imperfect detection from the user. Since we are interested in retrieving the photon from the emitter and a single pair from the SPDC source for entanglement swapping, under the loss model the resulting probabilities for $|\Psi_E\rangle$ and $|\Psi_P\rangle$ as defined in Equation (D1) and Equation (D2) are

$$\langle \Psi_E | \hat{\rho}_E | \Psi_E \rangle = \eta_e, \quad (\text{D10})$$

$$\langle \Psi_P | \hat{\rho}_{SPDC} | \Psi_P \rangle = \frac{\eta_s \eta_i \xi (\bar{\eta}_s \bar{\eta}_i \xi + 2)(1 - \xi)^2}{(1 - \bar{\eta}_s \bar{\eta}_i \xi)^4}, \quad (\text{D11})$$

where $\bar{\eta}_e = 1 - \eta_e$, $\bar{\eta}_s = 1 - \eta_s$, and $\bar{\eta}_i = 1 - \eta_i$.

b. Photodetector metrics

In this work, we provide practical estimates of the fidelity achievable using photon number-resolving detectors for entanglement swapping. We assume each detector in the setup has some efficiency η_{det} and also model dark counts which arise due to inherent electronic noise in a detector. Each dark count event is assumed to be independent and generated at a constant rate R_d cps, and typically dark count rates can be low ($< 10^{-2}$ cps) for single-photon detectors such as Transition Edge Sensors [70]. Furthermore, we assume the exposure time of the detectors, t_{exp} is much longer than the time scale over which dark counts emerge. The probability for n_d dark counts on a detector during each measurement cycle can then be approximated by a Poisson distribution [71]

$$P_d(n_d) = e^{-R_d t_{exp}} \frac{(R_d t_{exp})^{n_d}}{n_d!}. \quad (\text{D12})$$

The joint measurement in the heralding involves the use of detectors in output ports c and d in Figure 12. Therefore, we need to consider the effect of four detection outcomes for the herald – two detectors each with two orthonormal results, and the probability of dark counts for each. We assume identical dark count distributions for the detectors used in the herald.

c. Entanglement swapping and heralded success probability

A successful herald occurs at a probability which we define as P_s . For the HoD scheme, $P_s = \eta_e$ as we perform additional single and two-qubit operations on a graph only when the photon from the emitter is successfully measured. In the HoS scheme, P_s is the probability of detecting the set of detector click patterns requisite for the entanglement swap.

An extra source of infidelity for the heralded Bell state measurement occurs from the joint measurement itself. We define P_t as the overall probability of projecting the idler photon and emitter onto a Bell state for each joint measurement attempt. The probabilities are indicated in Figure 12(b). This will be a function of the detection efficiencies of the photons as well as the probability of zero dark count events detected. From Equation (D10), Equation (D11), and Equation (D12), P_t is given by

$$\begin{aligned} P_t(\eta_e, \eta_s, \eta_i, \xi) &= \frac{1}{2} \langle \Psi_E | \hat{\rho}_E | \Psi_E \rangle \langle \Psi_P | \hat{\rho}_{SPDC} | \Psi_P \rangle P_d^4(0) \\ &= \frac{1}{2} \frac{\eta_e \eta_s \eta_i \xi (\bar{\eta}_s \bar{\eta}_i \xi + 2)}{(1 - \bar{\eta}_s \bar{\eta}_i \xi)^4} (1 - \xi)^2 P_d^4(0). \end{aligned} \quad (\text{D13})$$

The heralded success probability P_s for the joint measurement is conditioned on a detection pattern representing the orthonormality of the photon states after the beamsplitter. This is a source of infidelity as the joint detection of states such as $|0; 0\rangle^{(p_e)} |1; 1\rangle^{(p_s)}$, representing two signal photons that are orthonormal to each other from the photon pair source and no photons from the emitter, possible due to detection or collection losses, would not result in entanglement swapping. We can identify the set of states that would result in a “success”:

$$S = \{|1; 0\rangle^{(p_e)} |0; 1\rangle^{(p_s)}, |0; 1\rangle^{(p_e)} |1; 0\rangle^{(p_s)}, |0; 0\rangle^{(p_e)} |1; 1\rangle^{(p_s)}\} \quad (\text{D14})$$

For each state in the set S , dark counts can lead to a false detection of the state. For example, the state $|1; 0\rangle^{(p_e)} |0; 1\rangle^{(p_s)}$ with zero dark counts is indistinguishable from the state $|1; 0\rangle^{(p_e)} |0; 0\rangle^{(p_s)}$ with one dark count falsely attributed to the measurement of a signal photon in the state $|0; 1\rangle^{(p_s)}$. The former has an additional associated dark count probability of $P_d^4(0)$ and the latter $P_d(1)P_d^3(0)$. Thus, we can compute P_s by considering the

probability of measuring all states in S and all dark count combinations and photon number states that reconstruct each element of S . By taking the partial trace of the emitter and idler photon from Equation (D7) and Equation (D8), and considering the probabilities mentioned in the overall set of joint measurement outcomes, we arrive at the probability P_s for the joint measurement,

$$\begin{aligned} P_s(\eta_e, \eta_s, \xi) &= \frac{3\bar{\eta}_e}{(1 - \bar{\eta}_s \xi)^2} (1 - \xi)^2 P_d^2(1) P_d^2(0) \\ &+ \left[\frac{\eta_e}{(1 - \bar{\eta}_s \xi)^2} + \frac{4\bar{\eta}_e \eta_s \xi}{(1 - \bar{\eta}_s \xi)^3} \right] (1 - \xi)^2 P_d(1) P_d^3(0) \\ &+ \left[\frac{\eta_e \eta_s \xi}{(1 - \bar{\eta}_s \xi)^3} + \frac{\bar{\eta}_e \eta_s^2 \xi^2}{(1 - \bar{\eta}_s \xi)^4} \right] (1 - \xi)^2 P_d^4(0). \end{aligned} \quad (\text{D15})$$

In this paper, we consider the case where heralding is repeated until a “success” is flagged for each idler photon added to the graph. Thus, the fidelity of the entanglement swapping procedure is $F_{\text{swap}} = P_t/P_s$.

d. Decoherence

The emitter used to generate photons, as well as any auxiliary spins entangled with an existing graph, will dephase across the duration until they are measured and projected back onto a known state. For an emitter or auxiliary spin represented by a density matrix $\hat{\rho}$, we model the dephasing process via the map

$$\hat{\rho} \rightarrow \mathcal{D}(\hat{\rho}; t, \tau) = \frac{1}{2}(1 + e^{-t/\tau})\hat{\rho} + \frac{1}{2}(1 - e^{-t/\tau})Z\hat{\rho}Z, \quad (\text{D16})$$

where τ is the coherence time of the emitter or auxiliary spin and t is a timescale for the dephasing process. Clearly this process leaves the state invariant with probability $\frac{1}{2}(1 + e^{-t/\tau})$, or conjugates it by Z with probability $\frac{1}{2}(1 - e^{-t/\tau})$. It is straightforward to verify that this map describes a Markovian process such that

$$\mathcal{D}(\hat{\rho}; t_1 + t_2, \tau) = \mathcal{D}(\hat{\rho}; t_2, \tau) \circ \mathcal{D}(\hat{\rho}; t_1, \tau). \quad (\text{D17})$$

We assume that each attempted herald happens on a short, regular timescale $t_{\text{rep}} = R_{\text{rep}}^{-1}$, which is simply the inverse repetition rate of the experiment. Furthermore, we assume each qubit gate operation time is near-instantaneous compared to t_{rep} , so that the dephasing takes place during the attempted herald only. As the emitter is measured out and reinitialized with each cycle of the experiment, it is evident that it will only dephase for at most t_{rep} . This implies that for each photon added to the graph, the contribution to the graph state fidelity from the decoherence of the emitter is $\frac{1}{2}(1 + e^{-t_{\text{rep}}/\tau_e})$, such that

$$F_D^{(e)}(n_p) = \left(\frac{1}{2} \left(1 + e^{-t_{\text{rep}}/\tau_e} \right) \right)^{n_p}, \quad (\text{D18})$$

is the total contribution towards building an n_p -photon graph state, and τ_e is the coherence time for the emitter.

We now model the contribution to the final state fidelity from any auxiliary spins in the system, which dephase for the entirety of their presence in the graph. Consider a mixed state density operator $\hat{\rho}_n = \sum_{\lambda} p_{\lambda} |\Phi_{\lambda}\rangle\langle\Phi_{\lambda}|$, described by a convex combination of n -qubit pure stabilizer states $|\Phi_{\lambda}\rangle$, where p_{λ} are the corresponding classical probabilities. This could represent the mixture of states one expects for an existing graph state built on a set of auxiliary spins, when under the action of its environment—including the prior action of the dephasing map itself. The system is initially stabilized by a set of generators $S_{|\Phi_{\lambda}\rangle} = \langle g_{1,\lambda}, g_{2,\lambda}, \dots, g_{n,\lambda} \rangle$. Under the dephasing map the state evolves as

$$\mathcal{D}^{(s)}(\hat{\rho}_n; t, \tau_s) = \frac{1}{2}(1 + e^{-t/\tau_s}) \sum_{\lambda} p_{\lambda} |\Phi_{\lambda}\rangle\langle\Phi_{\lambda}| + \frac{1}{2}(1 - e^{-t/\tau_s}) \sum_{\lambda} p_{\lambda} Z^{(s)} |\Phi_{\lambda}\rangle\langle\Phi_{\lambda}| Z^{(s)}, \quad (\text{D19})$$

which is once again a convex combination of stabilizer states with generators

$$\begin{aligned} S_{|\Phi_{\lambda}\rangle} &= \langle g_{1,\lambda}, g_{2,\lambda}, \dots, g_{n,\lambda} \rangle, \\ S_{Z^{(s)}|\Phi_{\lambda}\rangle} &= \langle Z^{(s)} g_{1,\lambda} Z^{(s)}, Z^{(s)} g_{2,\lambda} Z^{(s)}, \dots, Z^{(s)} g_{n,\lambda} Z^{(s)} \rangle. \end{aligned} \quad (\text{D20})$$

τ_s is the coherence time of the auxiliary spins in the system, which we treat as identical. Since we are interested in graph states, $\hat{\rho}_{G=(V,E)} = |G\rangle\langle G|$, whose stabilizers are generated by the operators $\{K_a\}_{a \in V}$ defined in Equation (A3),

the dephasing map only acts on the generators proportional to $X^{(s)}$, for any auxiliary spin (s) in the system. Hence, a graph state consisting of n_p photons and n_s auxiliary spins would evolve under the dephasing map as the mixture

$$\mathcal{D}^{(s)}(\hat{\rho}_G; t, \tau_s) = \sum_{\mathbf{b} \in \mathbb{Z}_2^{n_s}} p(\mathbf{b}) |G_{\mathbf{b}}\rangle\langle G_{\mathbf{b}}|, \quad (\text{D21})$$

where $\mathbf{b} = (b_1, b_2, \dots, b_{n_s}) \in \mathbb{Z}_2^{n_s}$ and

$$p(\mathbf{b}) = \frac{1}{2^{n_s}} \prod_{i=1}^{n_s} (1 + (-1)^{b_i} e^{-t/\tau_s}). \quad (\text{D22})$$

This mixture is stabilized by the set of generators,

$$S_{|G_{\mathbf{b}}\rangle} = \langle K_1^{(p)}, \dots, K_{n_p}^{(p)}, (-1)^{b_1} K_1^{(s)}, \dots, (-1)^{b_{n_s}} K_{n_s}^{(s)} \rangle. \quad (\text{D23})$$

The size of the system's stabilizer grows by one with each new photon m added to the graph. For the passing-subroutines we employ in Appendix C2, we apply this rule, however in choosing either variation of the subroutine we choose whether to rotate the auxiliary spin out of the basis of the dephasing map, and consequentially project the system onto a new mixed state as described above. That is for the m^{th} photon, we generate a new subgroup of the stabilizer as either

$$S_{|G\rangle, \text{join-}m} = \langle (-1)^{b_k} \dots Z_k^{(p)} \dots Z_m^{(p)} X^{(s)}, X_m^{(p)} Z^{(s)} \rangle, \quad (\text{D24a})$$

$$S_{|G\rangle, \text{extend-}m} = \langle (-1)^{b_k} \dots Z_k^{(p)} \dots X_m^{(p)} Z^{(s)}, Z_m^{(p)} X^{(s)} \rangle. \quad (\text{D24b})$$

Here, the bit conditioning phase b_k is applied to the generator $K^{(s)}$ during the creation of the k^{th} photon, with $k < m$. If we allow the system to continue dephasing, these subgroups evolve, distinctly, as

$$S_{|G_{\mathbf{b}}\rangle, \text{join-}m} = \langle (-1)^{b_k + b_m} \dots Z_k^{(p)} \dots Z_m^{(p)} X^{(s)}, X_m^{(p)} Z^{(s)} \rangle, \quad (\text{D25a})$$

$$S_{|G_{\mathbf{b}}\rangle, \text{extend-}m} = \langle (-1)^{b_k} \dots Z_k^{(p)} \dots X_m^{(p)} Z^{(s)}, (-1)^{b_m} Z_m^{(p)} X^{(s)} \rangle. \quad (\text{D25b})$$

We see that in the case of executing the extend-subroutine on m^{th} photon, the number of states in the mixture doubles, whereas in the case of the join-subroutine, the symmetry between states where either $b_k = b_m$ or $b_k \neq b_m$ leads to an effective mixture the same size as it was prior to the m^{th} photon's addition. Furthermore, we can express the probability for each state in the mixture in terms of b_k and b_m as

$$P(b_k, b_m) = \frac{1}{4} \left(1 + (-1)^{b_k} e^{-t_k/\tau_s} \right) \left(1 + (-1)^{b_m} e^{-t_m/\tau_s} \right). \quad (\text{D26})$$

where we have defined t_k and t_m as arbitrary times from the probabilistic nature of the herald. For the join-subroutine, the graph state remains unchanged when $b_k, b_m = 0$ or $b_k, b_m = 1$, whereas, for the extend-subroutine, the graph state remains unchanged only when $b_k, b_m = 0$. Hence, the fidelity under the dephasing model scales as $\frac{1}{2}(1 + e^{-(t_k + t_m)/\tau_s})$ for the join-subroutine and $\frac{1}{4}(1 + e^{-t_k/\tau_s})(1 + e^{-t_m/\tau_s})$ for the extend-subroutine for iterations k and m . This is a subtle distinction that arises from the Markovian nature of the dephasing map when implementing the join-subroutine. It implies the final state fidelity when constructing graph states on a set of auxiliary spins will in general depend on the sequence describing how each photon is passed into the system. In contrast, we assume $t_{\text{rep}} \ll \tau_s$ in our estimates, such that this distinction is not necessary, as $\frac{1}{4}(1 + e^{-t_k/\tau_s})(1 + e^{-t_m/\tau_s}) \approx \frac{1}{2}(1 + e^{-(t_k + t_m)/\tau_s})$. We provide estimates where t_{rep}/τ_s is of order $10^{-7} - 10^{-9}$ [12, 36]. It is nonetheless important to discuss, when considering auxiliary spins with shorter coherence times or constructing exceedingly large graph states, where the time to build the graph is of order the coherence time.

Lastly, we account for the probabilistic nature of the herald. Building graph states using either scheme we propose can be viewed as a Bernoulli trial with success probability P_s occurring at regular intervals t_{rep} . The cumulative probability that m trials yields r successes is given by the distribution

$$h(m, r, P_s) = \binom{m-1}{r-1} P_s^r (1 - P_s)^{m-r}, \quad (\text{D27})$$

where $m = r, r+1, r+2, \dots$. For any auxiliary spins in the graph, any failure to herald adds an additional t_{rep} to the dephasing time. Therefore, we model the mean contribution to the state fidelity for an auxiliary spin with r photons

passed to it under either passing-subroutine as

$$\begin{aligned}
\langle F_D^{(s)}(r, P_s) \rangle &= \sum_{m=r}^{\infty} h(m, r, P_s) \left(\frac{1}{2} \left(1 + e^{-mt_{\text{rep}}/\tau_s} \right) \right) \\
&= \frac{1}{2} \left(1 + \left(\frac{P_s}{P_s + e^{t_{\text{rep}}/\tau_s} - 1} \right)^r \right) \\
&\approx \frac{1}{2} \left(1 + e^{-rt_{\text{rep}}/P_s\tau_s} \right),
\end{aligned} \tag{D28}$$

where $\langle \dots \rangle$ here denotes a classical expectation value, and t_{rep}/P_s is the average time for a successful herald. Note in the HoD scheme, $P_s = \eta_e$, whereas in the HoS scheme it is of the form in Equation (D15). For an n_p -photon graph state, we take r up to the number of photons that a given auxiliary spin remains a part of the graph. Here, we consider the same coherence times for the emitter and auxiliary spins, $\tau_e = \tau_s = \tau$. Given state-of-the-art of trapped ion experiments [12], we take the dephasing timescale to be $t_{\text{rep}}/\tau = 10^{-9}$ in our best estimates.

e. Gates

Single-qubit gates applied to photons, the emitter and any auxiliary spins are assumed to be perfect in our model. For all two-qubit spin-spin entangling gates, we assume a fidelity $F_{CZ} = 0.999$ in our best estimates, in line with benchmarks from state-of-the-art trapped ion experiments [14, 15]. We assume the time to implement any single-qubit or two-qubit gate, $t_{\text{gate}} \ll t_{\text{rep}}$, and can therefore be treated as instantaneous.

f. Initial entanglement fidelity

In practice, there will be a non-unit fidelity on initializing the emitter onto the state described in Equation (D1) as well as Equation (D2) for the pair source. The additional contribution to the overall fidelity using our schemes, as compared to schemes where an emitter is directly used to generate graphs, is the entanglement fidelity of the nonlinear photon pair source in our HoS scheme. For example, the main contribution to the degradation of polarization-based entanglement fidelity for a single photon pair in SPDC comes from the spatial-temporal profile of the pump [72] and its interaction with the specific nonlinear medium, in which different spatial and spectral or temporal components impart different relative phases to the entangled pair described by Equation (D2). The fidelity can be optimized by using compensating crystals or filtering techniques; however, the latter also lowers the collection efficiency. Nevertheless, some of the best estimated fidelities for polarization-entangled SPDC sources range from $\sim 97\%$ to $\sim 99.7\%$ for various free-space and fiber-based setups [73–75]. In terms of overall fidelity estimations, we can introduce additional scaling terms similar to the gate fidelity described above. We denote the initial entanglement fidelities for the emitter photon and photon-photon pair as F_e and F_p , respectively. We focus primarily on the fidelity from the SPDC source to highlight the additional infidelity from our scheme.

3. Pair generation rate optimization

Given the infidelity from false heralds, defined in Equations (D13) and (D15), there exists a trade-off between the rate and fidelity at which large graph states can be generated in the HoS scheme, as set by the dimensionless parameter ξ , controlling the pair generation rate of the SPDC source. Decreasing ξ improves the probability of heralding a true Bell state, at the cost of longer average times between successful heralds. Conversely, the effects of decoherence on any auxiliary spins in the system, through Equation (D28), reduces the fidelity of the graph state, as the overall construction time increases. Hence, there is an optimum rate at which HoS can run, controlled by ξ and parameterized by the relevant total collection and detection efficiencies $\{\eta_e, \eta_s, \eta_i\}$, dark count rate, R_d , dephasing timescale, t_{rep}/τ , number of auxiliary spins, n_s , and total number of photons, n_p , required by the graph. Given a fixed set of parameters, this is a straightforward scalar maximization problem that can be accomplished numerically. If necessary, one can optimize within some ϵ of the optimum in order to achieve a speed-up in the rate.

4. Example applications

We briefly demonstrate how the sources of infidelity, presented in Appendix D 2, are combined to produce the fidelity estimates discussed in Sections IV and V. We note from the above that this fidelity is a mean estimate, optimized over ξ . For the estimates discussed in our work, we assume a negligible dark count rate, and let $\eta_s = \eta_i = 1$. In practice the signal photon collection efficiency can be near unity [36], and only makes a minor impact on the rate and fidelity that does not affect the overall scaling of either function, relative to the other relevant parameters. We carry out the optimization numerically, and determine ξ which achieves the optimum fidelity, when considering estimates in our HoS scheme.

a. GHZ states and cluster states

In Section IV, we present the mean final state fidelity to generate arbitrary graph states, requiring a single auxiliary spin in either of our schemes, such as the n_p -photon star graph, which is local-unitary equivalent to a GHZ state, or a 1D cluster state. For these graph states we optimize a function of the form

$$F_{n_s=1}(\xi; n_p, \eta_e) = (F_{\text{ent}} F_{\text{swap}}(\xi; \eta_e))^{n_p} F_D^{(e)}(n_p) \langle F_D^{(s)}(n_p, P_s(\eta_e, \xi)) \rangle. \quad (\text{D29})$$

Here, we have defined $F_{\text{ent}} = F_{CZ} F_p$ to combine the spin-spin entangling gate and photon pair entanglement fidelities, respectively. In Figure 4, we compare the effects of false heralds and decoherence against the limits imposed by imperfect spin-spin gate and initial SPDC photon pair entanglement fidelities, and hence set $F_{\text{ent}} = 1$ when computing estimates in the false herald and decoherence limited regimes. In the decoherence limited regime we additionally set $F_{\text{swap}} = 1$ and subsequently do not require optimization. Computing the fidelity to make these states in our schemes with perfect spin-spin entangling gates and initial photon pair entanglement assumes that additional error-correction or purification is employed.

b. Multi-party computation

For the MPC introduced in Section V, fidelity estimates for the generation of each 12-qubit graph state $|G\rangle$, depicted in Figure 5, are required to estimate the total bit error probability on the protocol. We assume graph states constructed in the HoD scheme discussed in Section III, where the computation of f happens in parallel with the construction of each state, and no pair source or photonic memory is required. In this scheme we take $P_s = \eta_e = 0.4$, from trapped ion experiments utilizing parabolic reflectors [19]. Additionally, we assume a dephasing timescale $t_{\text{rep}}/\tau = 10^{-9}$, following the best estimates for trapped ions [12]. The production of arbitrarily large graph states using our scheme is predominately limited by the spin-spin entangling gate fidelity and photon pair entanglement fidelity, F_{CZ} and F_p , respectively. From Equation (D18) and Equation (D28), the mean fidelity to produce each copy of the state is

$$F_G = F_{\text{ent}}^{12} F_{CZ}^5 F_D^{(e)}(12) \langle F_D^{(s_1)}(12, \eta_e) \rangle \langle F_D^{(s_2)}(4, \eta_e) \rangle^2, \quad (\text{D30})$$

where we have defined again $F_{\text{ent}} = F_{CZ} F_p$. We note additional spin-spin entangling gates are required to make this graph state, as compared to Equation (D29).

-
- [1] R. Raussendorf and H. J. Briegel, A one-way quantum computer, *Phys. Rev. Lett.* **86**, 5188 (2001).
 - [2] D. E. Browne and T. Rudolph, Resource-efficient linear optical quantum computation, *Phys. Rev. Lett.* **95**, 010501 (2005).
 - [3] N. H. Lindner and T. Rudolph, Proposal for pulsed on-demand sources of photonic cluster state strings, *Phys. Rev. Lett.* **103**, 113602 (2009).
 - [4] S. E. Economou, N. Lindner, and T. Rudolph, Optically generated 2-dimensional photonic cluster state from coupled quantum dots, *Phys. Rev. Lett.* **105**, 093601 (2010).
 - [5] A. Russo, E. Barnes, and S. E. Economou, Generation of arbitrary all-photonic graph states from quantum emitters, *New Journal of Physics* **21**, 055002 (2019).
 - [6] P. Hilaire, L. Vidro, H. S. Eisenberg, and S. E. Economou, Near-deterministic hybrid generation of arbitrary photonic graph states using a single quantum emitter and linear optics, *Quantum* **7**, 992 (2023).
 - [7] Y. Meng, C. F. Faurby, M. L. Chan, P. I. Sund, Z. Liu, Y. Wang, N. Bart, A. D. Wieck, A. Ludwig, L. Midolo,

- et al.*, Photonic fusion of entangled resource states from a quantum emitter, arXiv preprint arXiv:2312.09070 (2023).
- [8] P. Thomas, L. Ruscio, O. Morin, and G. Rempe, Fusion of deterministically generated photonic graph states, *Nature*, 1 (2024).
- [9] Y. Zhan and S. Sun, Deterministic generation of loss-tolerant photonic cluster states with a single quantum emitter, *Physical Review Letters* **125**, 223601 (2020).
- [10] D. Cogan, Z.-E. Su, O. Kenneth, and D. Gershoni, Deterministic generation of indistinguishable photons in a cluster state, *Nature Photonics* **17**, 324–329 (2023).
- [11] D. Bluvstein, H. Levine, G. Semeghini, T. T. Wang, S. Ebadi, M. Kalinowski, A. Keesling, N. Maskara, H. Pichler, M. Greiner, V. Vuletić, and M. D. Lukin, A quantum processor based on coherent transport of entangled atom arrays, *Nature* **604**, 451–456 (2022).
- [12] P. Wang, C.-Y. Luan, M. Qiao, M. Um, J. Zhang, Y. Wang, X. Yuan, M. Gu, J. Zhang, and K. Kim, Single ion qubit with estimated coherence time exceeding one hour, *Nature communications* **12**, 1 (2021).
- [13] S. J. Evered, D. Bluvstein, M. Kalinowski, S. Ebadi, T. Manovitz, H. Zhou, S. H. Li, A. A. Geim, T. T. Wang, N. Maskara, H. Levine, G. Semeghini, M. Greiner, V. Vuletić, and M. D. Lukin, High-fidelity parallel entangling gates on a neutral-atom quantum computer, *Nature* **622**, 268–272 (2023).
- [14] R. Srinivas, S. C. Burd, H. M. Knaack, R. T. Sutherland, A. Kwiatkowski, S. Glancy, E. Knill, D. J. Wineland, D. Leibfried, A. C. Wilson, D. T. C. Allcock, and D. H. Slichter, High-fidelity laser-free universal control of trapped ion qubits, *Nature* **597**, 209–213 (2021).
- [15] C. R. Clark, H. N. Tinkey, B. C. Sawyer, A. M. Meier, K. A. Burkhardt, C. M. Seck, C. M. Shappert, N. D. Guise, C. E. Volin, S. D. Fallek, H. T. Hayden, W. G. Rellergert, and K. R. Brown, High-fidelity bell-state preparation with $^{40}\text{Ca}^+$ optical qubits, *Physical Review Letters* **127**, 10.1103/physrevlett.127.130505 (2021).
- [16] G. Shu, C.-K. Chou, N. Kurz, M. R. Dietrich, and B. B. Blinov, Efficient fluorescence collection and ion imaging with the “tack” ion trap, *J. Opt. Soc. Am. B* **28**, 2865 (2011).
- [17] D. Hucul, I. V. Inlek, G. Vittorini, C. Crocker, S. Debath, S. M. Clark, and C. Monroe, Modular entanglement of atomic qubits using photons and phonons, *Nature Physics* **11**, 37 (2015).
- [18] C.-K. Chou, C. Aughter, J. Lilieholm, K. Smith, and B. Blinov, Note: Single ion imaging and fluorescence collection with a parabolic mirror trap, *Review of Scientific Instruments* **88** (2017).
- [19] R. Maiwald, A. Golla, M. Fischer, M. Bader, S. Heugel, B. Chalopin, M. Sondermann, and G. Leuchs, Collecting more than half the fluorescence photons from a single ion, *Physical Review A* **86**, 043431 (2012).
- [20] P. Thomas, L. Ruscio, O. Morin, and G. Rempe, Efficient generation of entangled multiphoton graph states from a single atom, *Nature* **608**, 677 (2022).
- [21] J. Schupp, V. Krucmarsky, V. Krutyanskiy, M. Meraner, T. Northup, and B. Lanyon, Interface between trapped-ion qubits and traveling photons with close-to-optimal efficiency, *PRX Quantum* **2**, 020331 (2021).
- [22] X. Ding, Y.-P. Guo, M.-C. Xu, R.-Z. Liu, G.-Y. Zou, J.-Y. Zhao, Z.-X. Ge, Q.-H. Zhang, H.-L. Liu, M.-C. Chen, *et al.*, High-efficiency single-photon source above the loss-tolerant threshold for efficient linear optical quantum computing, arXiv preprint arXiv:2311.08347 (2023).
- [23] A. Kinos, D. Hunger, R. Kolesov, K. Mølmer, H. de Riedmatten, P. Goldner, A. Tallaire, L. Morvan, P. Berger, S. Welinski, *et al.*, Roadmap for rare-earth quantum computing, arXiv preprint arXiv:2103.15743 (2021).
- [24] R. Yanagimoto, R. Nehra, R. Hamerly, E. Ng, A. Marandi, and H. Mabuchi, Quantum nondemolition measurements with optical parametric amplifiers for ultrafast universal quantum information processing, *PRX Quantum* **4**, 010333 (2023).
- [25] S. E. Economou, L. J. Sham, Y. Wu, and D. G. Steel, Proposal for optical u(1) rotations of electron spin trapped in a quantum dot, *Phys. Rev. B* **74**, 205415 (2006).
- [26] M. Gimeno-Segovia, T. Rudolph, and S. E. Economou, Deterministic generation of large-scale entangled photonic cluster state from interacting solid state emitters, *Phys. Rev. Lett.* **123**, 070501 (2019).
- [27] D. Rieländer, A. Lenhard, M. Mazzera, and H. De Riedmatten, Cavity enhanced telecom heralded single photons for spin-wave solid state quantum memories, *New Journal of Physics* **18**, 123013 (2016).
- [28] J. P. Covey, H. Weinfurter, and H. Bernien, Quantum networks with neutral atom processing nodes, *npj Quantum Information* **9**, 10.1038/s41534-023-00759-9 (2023).
- [29] T. Ward and M. Keller, Generation of time-bin-encoded photons in an ion-cavity system, *New Journal of Physics* **24**, 123028 (2022).
- [30] V. Krutyanskiy, M. Galli, V. Krucmarsky, S. Baier, D. A. Fioretto, Y. Pu, A. Mazloom, P. Sekatski, M. Canteri, M. Teller, J. Schupp, J. Bate, M. Meraner, N. Sangouard, B. P. Lanyon, and T. E. Northup, Entanglement of trapped-ion qubits separated by 230 meters, *Phys. Rev. Lett.* **130**, 050803 (2023).
- [31] H. Jayakumar, A. Predojević, T. Kauten, T. Huber, G. S. Solomon, and G. Weihs, Time-bin entangled photons from a quantum dot, *Nature Communications* **5**, 10.1038/ncomms5251 (2014).
- [32] P. Senellart, G. Solomon, and A. White, High-performance semiconductor quantum-dot single-photon sources, *Nature Nanotechnology* **12**, 1026–1039 (2017).
- [33] J. Schneeloch, S. H. Knarr, D. F. Bogorin, M. L. Levangie, C. C. Tison, R. Frank, G. A. Howland, M. L. Fanto, and P. M. Alsing, Introduction to the absolute brightness and number statistics in spontaneous parametric down-conversion, *Journal of Optics* **21**, 043501 (2019).
- [34] C. Zhang, Y.-F. Huang, B.-H. Liu, C.-F. Li, and G.-C. Guo, Spontaneous parametric down-conversion sources for multiphoton experiments, *Advanced Quantum Technologies* **4**, 2000132 (2021).
- [35] J.-W. Pan, D. Bouwmeester, H. Weinfurter, and A. Zeilinger, Experimental entanglement swapping: entangling photons that never interacted, *Physical review letters* **80**, 3891 (1998).
- [36] S. Ramelow, A. Mech, M. Giustina, S. Gröblacher, W. Wieczorek, J. Beyer, A. Lita, B. Calkins, T. Gerrits, S. W. Nam, *et al.*, Highly efficient heralding of entangled single photons, *Optics express* **21**, 6707 (2013).
- [37] B. Li, S. E. Economou, and E. Barnes, Photonic resource state generation from a minimal number of quantum emitters, *npj Quantum Information* **8**, 10.1038/s41534-022-00522-6 (2022).
- [38] A. Lamas-Linares, J. C. Howell, and D. Bouwmeester,

- Stimulated emission of polarization-entangled photons, *Nature* **412**, 887 (2001).
- [39] N. Sangouard, B. Sanguinetti, N. Curtz, N. Gisin, R. Thew, and H. Zbinden, Faithful entanglement swapping based on sum-frequency generation, *Physical review letters* **106**, 120403 (2011).
- [40] D. L. P. Vitullo, M. G. Raymer, B. J. Smith, M. Karpiński, L. Mejling, and K. Rottwitt, Entanglement swapping for generation of heralded time-frequency-entangled photon pairs, *Phys. Rev. A* **98**, 023836 (2018).
- [41] H.-S. Zhong, Y. Li, W. Li, L.-C. Peng, Z.-E. Su, Y. Hu, Y.-M. He, X. Ding, W. Zhang, H. Li, L. Zhang, Z. Wang, L. You, X.-L. Wang, X. Jiang, L. Li, Y.-A. Chen, N.-L. Liu, C.-Y. Lu, and J.-W. Pan, 12-photon entanglement and scalable scattershot boson sampling with optimal entangled-photon pairs from parametric down-conversion, *Phys. Rev. Lett.* **121**, 250505 (2018).
- [42] M. Houshmand, M. Houshmand, and J. F. Fitzsimons, Minimal qubit resources for the realization of measurement-based quantum computation, *Phys. Rev. A* **98**, 012318 (2018).
- [43] R. Raussendorf, D. E. Browne, and H. J. Briegel, Measurement-based quantum computation on cluster states, *Phys. Rev. A* **68**, 022312 (2003).
- [44] D. E. Browne, E. Kashefi, M. Mhalla, and S. Perdrux, Generalized flow and determinism in measurement-based quantum computation, *New Journal of Physics* **9**, 250–250 (2007).
- [45] M. Varnava, D. E. Browne, and T. Rudolph, Loss tolerance in one-way quantum computation via counterfactual error correction, *Physical Review Letters* **97**, 10.1103/physrevlett.97.120501 (2006).
- [46] M. Pant, D. Towsley, D. Englund, and S. Guha, Percolation thresholds for photonic quantum computing, *Nature communications* **10**, 1070 (2019).
- [47] S. Bartolucci, P. Birchall, H. Bombín, H. Cable, C. Dawson, M. Gimeno-Segovia, E. Johnston, K. Kieling, N. Nickerson, M. Pant, F. Pastawski, T. Rudolph, and C. Sparrow, Fusion-based quantum computation, *Nature Communications* **14**, 10.1038/s41467-023-36493-1 (2023).
- [48] M. C. Löbl, S. Paesani, and A. S. Sørensen, Loss-tolerant architecture for quantum computing with quantum emitters, *Quantum* **8**, 1302 (2024).
- [49] R. Reichle, D. Leibfried, E. Knill, J. Britton, R. B. Blakestad, J. D. Jost, C. Langer, R. Ozeri, S. Seidelin, and D. J. Wineland, Experimental purification of two-atom entanglement, *Nature* **443**, 838 (2006).
- [50] M. D. Eisaman, J. Fan, A. Migdall, and S. V. Polyakov, Invited review article: Single-photon sources and detectors, *Review of scientific instruments* **82**, 071101 (2011).
- [51] A. C. Yao, Protocols for secure computations, in *23rd Annual Symposium on Foundations of Computer Science (sfcs 1982)* (1982) pp. 160–164.
- [52] O. Goldreich, S. Micali, and A. Wigderson, How to play any mental game, in *Proceedings of the nineteenth annual ACM conference on Theory of computing - STOC '87*, STOC '87 (ACM Press, 1987).
- [53] C. Zhao, S. Zhao, M. Zhao, Z. Chen, C.-Z. Gao, H. Li, and Y.-a. Tan, Secure multi-party computation: Theory, practice and applications, *Information Sciences* **476**, 357–372 (2019).
- [54] D. Beaver, Efficient multiparty protocols using circuit randomization, in *Lecture Notes in Computer Science* (Springer Berlin Heidelberg, 1992) p. 420–432.
- [55] J. B. Nielsen, P. S. Nordholt, C. Orlandi, and S. S. Burra, A new approach to practical active-secure two-party computation, in *Advances in Cryptology – CRYPTO 2012* (Springer Berlin Heidelberg, 2012) p. 681–700.
- [56] I. Damgård, V. Pastro, N. Smart, and S. Zakarias, Multiparty computation from somewhat homomorphic encryption, in *Advances in Cryptology – CRYPTO 2012* (Springer Berlin Heidelberg, 2012) p. 643–662.
- [57] A. Choudhury and A. Patra, An efficient framework for unconditionally secure multiparty computation, *IEEE Transactions on Information Theory* **63**, 428–468 (2017).
- [58] Y. Takeuchi, A. Mantri, T. Morimae, A. Mizutani, and J. Fitzsimons, Resource-efficient verification of quantum computing using serfling’s bound, *npj Quantum Information* **5**, 10.1038/s41534-019-0142-2 (2019).
- [59] A. Unnikrishnan and D. Markham, Verification of graph states in an untrusted network, *Phys. Rev. A* **105**, 052420 (2022).
- [60] S. Meesala, S. Wood, D. Lake, P. Chiappina, C. Zhong, A. D. Beyer, M. D. Shaw, L. Jiang, and O. Painter, Non-classical microwave-optical photon pair generation with a chip-scale transducer, *Nature Physics* , 1 (2024).
- [61] S. Mittal, V. V. Orre, A. Restelli, R. Salem, E. A. Goldschmidt, and M. Hafezi, Temporal and spectral manipulations of correlated photons using a time lens, *Physical Review A* **96**, 043807 (2017).
- [62] K.-H. Luo, H. Herrmann, S. Krapick, B. Brecht, R. Ricken, V. Quiring, H. Suche, W. Sohler, and C. Silberhorn, Direct generation of genuine single-longitudinal-mode narrowband photon pairs, *New Journal of Physics* **17**, 073039 (2015).
- [63] M. Hein, J. Eisert, and H. J. Briegel, Multiparty entanglement in graph states, *Phys. Rev. A* **69**, 062311 (2004).
- [64] E. B. Davies and J. T. Lewis, An operational approach to quantum probability, *Communications in Mathematical Physics* **17**, 239–260 (1970).
- [65] F. Baccari, R. Augusiak, I. Šupić, J. Tura, and A. Acín, Scalable bell inequalities for qubit graph states and robust self-testing, *Physical Review Letters* **124**, 10.1103/physrevlett.124.020402 (2020).
- [66] C. Schön, E. Solano, F. Verstraete, J. I. Cirac, and M. M. Wolf, Sequential generation of entangled multi-qubit states, *Physical Review Letters* **95**, 10.1103/physrevlett.95.110503 (2005).
- [67] S. L. Braunstein and A. Mann, Measurement of the bell operator and quantum teleportation, *Phys. Rev. A* **51**, R1727 (1995).
- [68] P. Kok and S. L. Braunstein, Postselected versus non-postselected quantum teleportation using parametric down-conversion, *Phys. Rev. A* **61**, 042304 (2000).
- [69] U. Leonhardt and H. Paul, Measuring the quantum state of light, *Progress in Quantum Electronics* **19**, 89 (1995).
- [70] R. Shah, K.-S. Isleif, F. Januschek, A. Lindner, and M. Schott, Characterising a single-photon detector for alps ii, *Journal of Low Temperature Physics* **209**, 355–362 (2022).
- [71] H. Lee, U. Yurtsever, P. Kok, G. M. Hockney, C. Adami, S. L. Braunstein, and J. P. Dowling, Towards photostatistics from photon-number discriminating detectors, *Journal of Modern Optics* **51**, 1517 (2004).
- [72] R. Rangarajan, M. Goggin, and P. Kwiat, Optimizing type-i polarization-entangled photons, *Opt. Express* **17**, 18920 (2009).

- [73] M. V. Jabir and G. K. Samanta, Robust, high brightness, degenerate entangled photon source at room temperature, *Scientific Reports* **7**, 12613 (2017).
- [74] F. Steinlechner, S. Ramelow, M. Jofre, M. Gilaberte, T. Jennewein, J. P. Torres, M. W. Mitchell, and V. Pruneri, Phase-stable source of polarization-entangled photons in a linear double-pass configuration, *Opt. Express* **21**, 11943 (2013).
- [75] M. Medic, J. B. Altepeter, M. A. Hall, M. Patel, and P. Kumar, Fiber-based telecommunication-band source of degenerate entangled photons, *Opt. Lett.* **35**, 802 (2010).